NASA Technical Memorandum 100955

Analysis and Optimization of Truncated Scarf Nozzles Subject to External Flow Conditions

Rickey J. Shyne
Lewis Research Center
Cleveland, Ohio

August 1988

NASA

ANALYSIS AND OPTIMIZATION OF TRUNCATED SCARF NOZZLES SUBJECT TO EXTERNAL FLOW CONDITIONS

Rickey J. Shyne
National Aeronautics and Space Administration
Lewis Research Center
Cleveland, Ohio 44135

SUMMARY

Results of a calculation of an optimized truncated scarfed nozzle were compared. The truncated scarfed nozzle was designed for an exit Mach number of 6.0, i.e., the Mach number at the last nozzle characteristic is 6.0, with an external flow Mach number of 5.0. The nozzle was designed by the Rao method for optimum thrust nozzles modified for two-dimensional flow and truncated scarfed nozzle applications. This design was analyzed using a shock-fitting method for two-dimensional supersonic flows.

Excellent agreement was achieved between the design and analysis. Truncation of the lower nozzle wall (cowl) revealed that there is an optimum length for truncating the cowl without degrading the nozzle performance. Truncation of the nozzle cowl past this optimal length should be analyzed in trade-off studies for thrust loss versus gross vehicle weight.

Plots of the oblique shock wave equations were also identified which will allow computation of slip line angle, dynamic pressure coefficient, or ambient Mach number for various specific heat ratios.

E-4146

TABLE OF CONTENTS

NOMENCLATURE

a speed of sound

A coefficient in finite difference equations and cross-sectional area

AR area ratio, A_e/A_t

C characteristic curve

C thrust coefficient - $\frac{\mathcal{F}}{\frac{1}{2}\rho V^2 A}$

f function

I integral

L length, inches

$\dot{m}$ mass flow rate

M Mach number

P static pressure

P total pressure

q dynamic pressure

Q coefficient in finite difference equations

r radial distance

R coefficient in finite difference equations

R_g gas constant

s distance

S coefficient in finite difference equations

t time

T temperature and coefficient in finite difference equations

$\mathcal{F}$ thrust

u velocity in x-direction

v velocity in y-direction

x Cartesian coordinate

y Cartesian coordinate

z axial distance

Greek Symbols

γ ratio of specific heats

δ slip line angle, first variational operator, and coefficient in two-dimensional flow equations

ε oblique shock wave angle

λ Lagrangian multiplier and slope of characteristic curve

μ Mach angle

ν Prandtl-Meyer expansion angle

ϕ control surface angle

ρ density

θ oblique shock wave angle

Subscripts

a ambient

e exit

PM Prandtl-Meyer

s shock

sl slip line

t throat

T total

+ left-running characteristic

- right-running characteristic

o streamline

INTRODUCTION

In the design of jet aircraft, it is desirable to design for optimum thrust while restricting the length of the exhaust nozzle for overall vehicle weight reduction. In recent years, interest in hypersonic and supersonic cruise vehicles has grown and presently studies are being performed to evaluate the feasibility of such vehicles. Exhaust nozzles designed for vehicles such as the high-speed civil transport (Orient Express) will have to be optimized for thrust while conforming to weight limits and other constraints imposed by particular missions.

Early attempts to design optimum thrust nozzles focused on the truncation of perfect nozzles. A perfect nozzle was designed for a uniform exit velocity. This nozzle was then truncated at a given area ratio. This process was repeated for designs with different uniform exit velocities. Each truncation then provided a nozzle with a different length for the desired area ratio. Examination of the thrust versus length or weight considerations provided the basis of selection of the desired optimal design.

Later attempts to design optimal nozzles involved the analysis of a family of assumed shapes. A shape such as a parabolic contour was assumed with a prescribed initial expansion angle and exit lip angle.

The angles were varied to provide a family of nozzle shapes. These nozzles were then analyzed to determine the performance and the optimal shape was therefore determined.

A method for designing an optimum thrust nozzle was developed by Rao (1958) in which variational calculus and the method of characteristics are used to compute the contour. The Rao optimization technique is unique in that it does not depend on a preselected family of mathematical functions for the contour and proceeds to find the optimal wall contour within that family. The Rao method determines the unique contour which yields the maximum thrust from the infinite array of possible contours. It does not necessarily determine a contour which can be specified by a simple mathematical equation.

The Rao method was incorporated into a computer program by Nickerson (1982). The code computes a nozzle contour of optimum thrust (1) for a given length, or (2) for a given area ratio, or (3) for both fixed length and exit plane radius. The Rao method was originally formulated for axisymmetric nozzles with circular throats as illustrated in Fig. 1. However, because of the renewed interest in high-speed aircraft the method was modified to compute two-dimensional, flat rectangular throat nozzles which can be used in ramjet engine applications. Such a nozzle is shown in Fig. 2. The method was also applied to designs where the lower nozzle wall (cowl) is terminated at the point where the last characteristic that emanates from the upper nozzle wall (ramp) intersects the cowl. This defines a two-dimensional, nonsymmetric nozzle as shown in Fig. 2. The flat throat

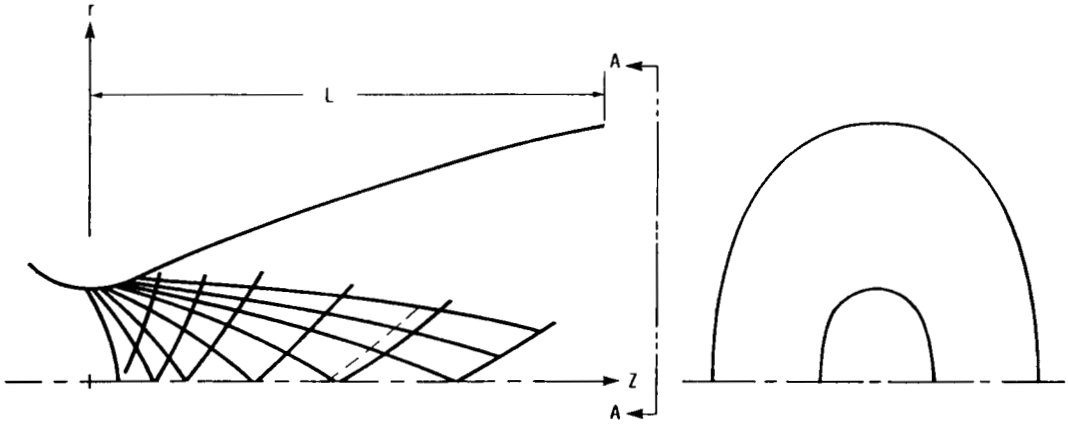

FIG. 1. - SCHEMATIC OF AN AXISYMMETRIC RAO NOZZLE

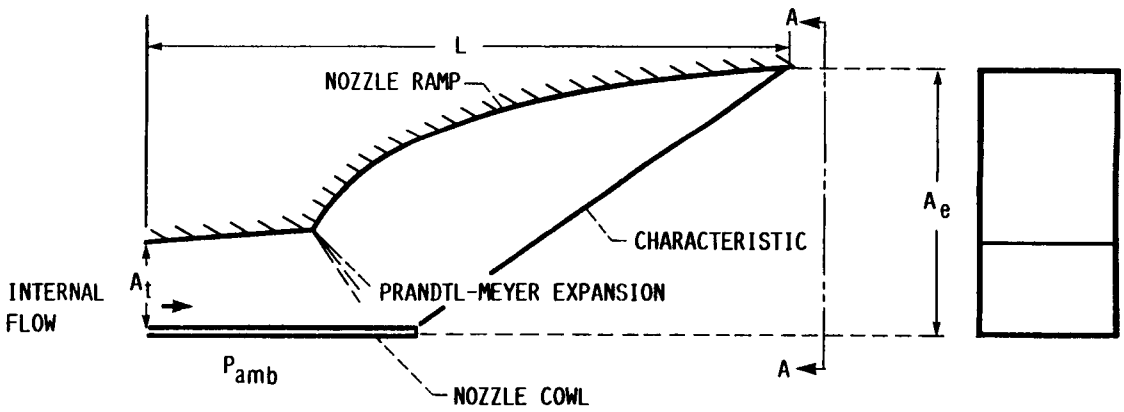

FIG. 2. - SCHEMATIC OF A TWO-DIMENSIONAL RAO NOZZLE WITH FLAT-THROAT MOODIFICATION

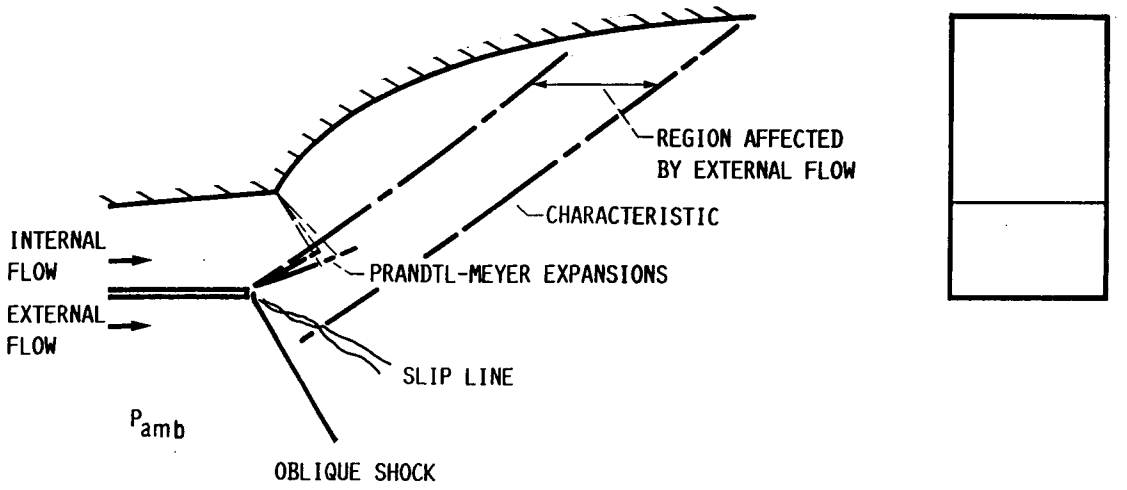

FIG. 3. - SCHEMATIC OF A TWO-DIMENSIONAL TRUNCATED RAO SCARFED NOZZLE

modification assumes an initial expansion of uniform flow followed by a Prandtl-Meyer expansion at the beginning of the turning section.

Significantly reduced vehicle weights can be obtained with two-dimensional, nonsymmetric nozzles and further weight reduction can be achieved by truncating the nozzle cowl upstream of the last nozzle ramp characteristic. However, because of the truncation, the design of the nozzle contour will be affected by the external flow as illustrated in Fig. 3. If the nozzle flow is underexpanded, an oblique shock wave and slip line will form at the exit because of the interaction of the external and internal flows.

The incorporation of external flow considerations into the optimization of exhaust nozzle contours defines the problem that is studied in this thesis. The objective of this work is to present a design method that may be used to compute optimized truncated scarfed nozzles and to present results of a parametric investigation that employs this method.

ANALYSIS

Rao Method

A procedure for computing axisymmetric, optimum thrust exhaust nozzle contours was developed by Rao (1958). This method defines a nozzle contour for an ideal gas with constant specific heats in an isentropic flow. For this method, a control surface is defined at the exit of the nozzle. The thrust is maximized such that the flow and length of the nozzle are fixed constraints. The solution of the external problem and the flow within the nozzle are then found by using the method of characteristics. This procedure was recently converted into a computer program by Nickerson (1982).

Figure 4 is a schematic of the top portion of a two-dimensional, axisymmetric nozzle contour with the characteristic net and control surface used for this analysis superimposed upon it. Line CE, in Fig. 4 describes the control surface having an angle of inclination ϕ to the axis. Figure 5 is a differential element of the control surface showing flow across it. Calculating the mass flow through this differential element yields (1)

$$d\dot{m} = \rho v \sin(\phi - \theta)\, dA. \tag{1}$$

where $dA = 2\pi r\, ds$ and $ds = dr/\sin\phi$. To obtain the mass flow crossing the control surface, the differential mass flow rate in Eq. (1) is integrated along line CE

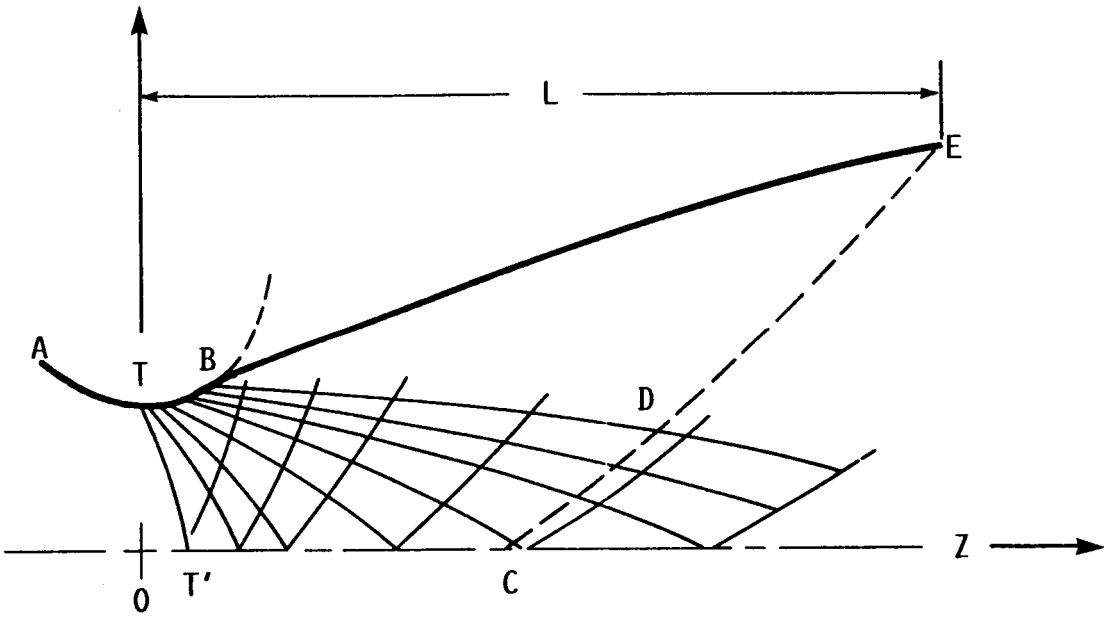

FIG. 4. - SCHEMATIC OF A RAO NOZZLE WITH CHARACTERISTIC NET AND CONTROL SURFACE

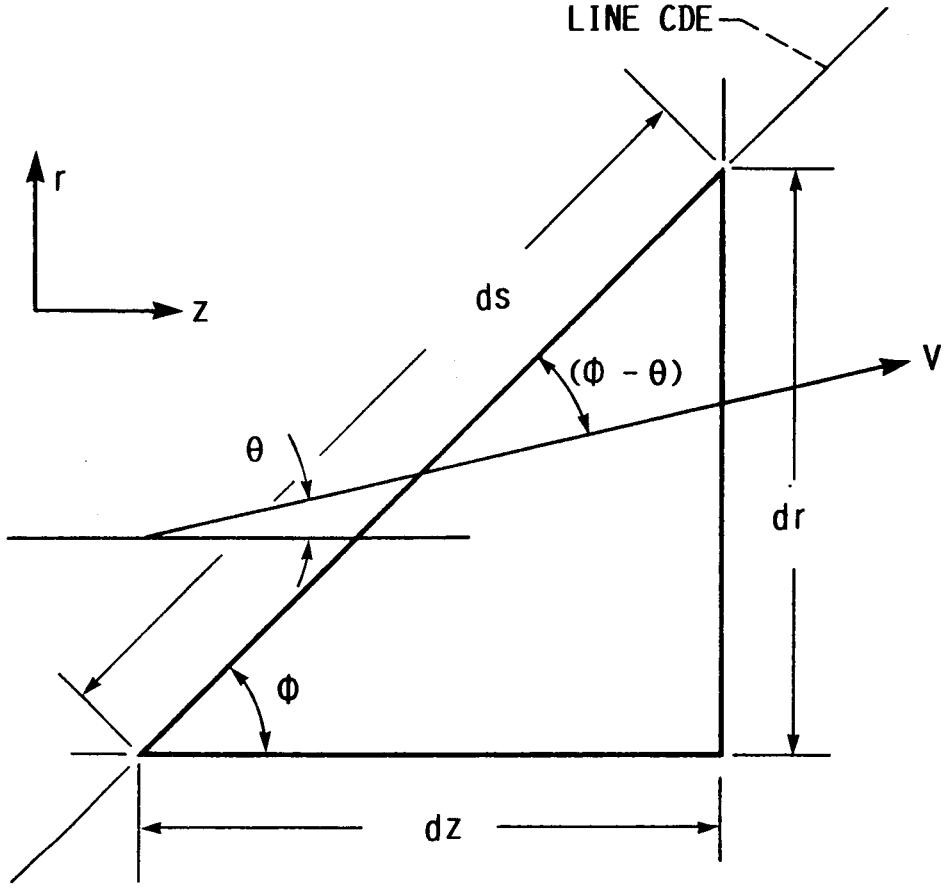

FIG. 5. - DIAGRAM OF A DIFFERENTIAL ELEMENT OF CONTROL SURFACE

$$\dot{m} = \int_C^E \rho v \frac{\sin(\phi - \theta)}{\sin \phi} 2\pi r \, dr. \tag{2}$$

The linear momentum flux in the z-direction is:

$$\text{momentum flux} = \rho v^2 \frac{\sin(\phi - \theta) \cos \theta}{\sin \phi} 2\pi r \, dr. \tag{3}$$

Computing the thrust on the nozzle yields

$$\mathcal{T} = \int_C^E \left[(p - p_a) + \rho v^2 \frac{\sin(\phi - \theta) \cos \theta}{\sin \phi}\right] 2\pi r \, dr. \tag{4}$$

The length of the nozzle is computed from

$$L = z_c + \int_C^E \cot \phi \, dr. \tag{5}$$

For a fixed throat contour the length of the nozzle to point C, z_c, is also fixed by the application of the entrance flow character and the solution of the flow equations. Hence the length constraint becomes

$$\int_C^E \cot \phi \, dr = \text{constant}. \tag{6}$$

Utilizing the Lagrangian multiplier method developed in Hildebrand (1976) and reviewed in Appendix A, the problem can now be reduced to maximizing the following integral:

$$I = \int_C^E (f_1 + \lambda_2 f_2 + \lambda_3 f_3) \, dr \tag{7}$$

where

$$f_1 = \left[(p - p_a) + \rho v^2 \frac{\sin(\phi - \theta)}{\sin \phi}\right] r \tag{8}$$

$$f_2 = \rho v \frac{\sin(\phi - \theta)}{\sin \phi} r \tag{9}$$

$$f_3 = \cot \phi. \tag{10}$$

Variational calculus principles reviewed in appendix B can now be applied to Eq. (7). Maximizing I requires that the first variation of the integral must be equal to zero. In turn, this will lead to an expression for the control surface and the flow conditions along it. The variation of I depends upon the optimization required. If the thrust is maximized such that the length is constant but the area ratio varies, then the upper limit of the integral is a variable and contributes to the variation of I. The variation of I does not depend on the lower limit. This can be illustrated by considering that the integral between limits of points C and E can be expressed as the sum of two integrals. One integral for the region between points C and D and the other integral for the region between points D and E. Since the throat contour is fixed, and hence, so is the resultant flow the variation of the integral with the limits of points C and E vanishes. Examining all possible variations of the quantities in I, the following set of possibilities are derived:

(1) δC, δM, $\delta \theta$, and $\delta \phi$ are zero along CD, since this portion of the flowfield is fixed by the specification of the throat contour.

(2) δM, $\delta \theta$, and $\delta \phi$ are nonzero along DE.

(3) At E, δz_E is zero, but δr_E is nonzero.

(4) Since M and θ are continuous along CE, then δD, although nonzero, does not enter into the first variation of I.

Performing the first variation of the integral I, results in

$$\delta I = 0 = \int_{r_D}^{r_E} \left\{ \left(f_{1_M} + \lambda_2 f_{2_M} + \lambda_3 f_{3_M} \right) \delta M + \left(f_{1_\theta} + \lambda_2 f_{2_\theta} + \lambda_3 f_{3_\theta} \right) \delta\theta \right.$$

$$\left. + \left(f_{1_\phi} + \lambda_2 f_{2_\phi} + \lambda_3 f_{3_\phi} \right) \delta\phi \right\} dr + \delta r_E \left(f_2 + \lambda_2 f_2 + \lambda_2 f_3 \right)_{\text{at } E} \qquad (11)$$

where the subscripts M, θ, and ϕ denote partial derivatives and δ is the variational operator. Since the variations in δM, $\delta\theta$, $\delta\phi$, and δr_E are arbitrary, each of their coefficients must be equal to zero, thus,

$$f_{1_M} + \lambda_2 f_{2_M} + \lambda_3 f_{3_M} = 0 \qquad (12)$$

$$f_{1_\theta} + \lambda_2 f_{2_\theta} + \lambda_3 f_{3_\theta} = 0 \qquad (13)$$

$$f_{1_\phi} + \lambda_2 f_{2_\phi} + \lambda_3 f_{3_\phi} = 0 \qquad (14)$$

along line DE, and

$$f_1 + \lambda_2 f_2 + \lambda_3 f_3 = 0 \quad \text{at} \quad E. \qquad (15)$$

If radial and axial distances at point E are both specified, the upper limit is fixed and the last term in Eq. (11) disappears from the variational solution. Since $f_{3_M} = f_{3_\theta} = 0$, these terms may be eliminated from Eqs. (12) and (13) and the two resulting equations are combined to give

$$f_{1_M} f_{2_\theta} = f_{1_\theta} f_{2_M} \, . \qquad (16)$$

The density, pressure, and velocity can be considered functions of Mach number for isentropic flow and can be computed from isentropic flow relations e.g., see Shapiro (1953) or John (1969). These relations are

$$\frac{\rho}{\rho_T} = \left(1 + \frac{\gamma - 1}{2} M^2\right)^{-1/\gamma-1} \tag{17}$$

$$\frac{p}{P_T} = \left(1 + \frac{\gamma - 1}{2} M^2\right)^{-\gamma/\gamma-1} \tag{18}$$

$$v = M\gamma^{1/2} \left(1 + \frac{\gamma - 1}{2} M^2\right)^{-1/2} . \tag{19}$$

Note, the static parameters have been nondimensionalized with respect to the total conditions. Utilizing Eqs. (17) to (19), it follows that

$$p_M = - \frac{\rho v^2}{M} \tag{20}$$

$$\rho_M = -pM \tag{21}$$

$$v_M = \frac{v}{M\left(1 + \frac{\gamma - 1}{2} M^2\right)} . \tag{22}$$

(Equations 20 and 21 are nondimensionalized to total conditions and $p_M = d(p/p_T)/dM$, $\rho_M = d\rho/dM$, and $v_M = dv/dM$). The partial derivatives f_{1_M} and f_{2_M} are determined from Eqs. (8) and (9) to give:

$$f_{1_M} = \left[- \frac{pv^2}{M} + \frac{2\rho v^2 \sin(\phi - \theta) \cos\theta}{M\left(1 + \frac{\gamma - 1}{2} M^2\right)\sin\phi} - \frac{v^2 Mp \sin(\phi - \theta) \cos\theta}{\sin\phi} \right] r \tag{23}$$

and

$$f_{2_M} = \frac{\sin(\phi - \theta)}{\sin \phi} r \left[\frac{\rho v}{M\left(1 + \frac{\gamma - 1}{2} M^2\right)} - vMp \right] \tag{24}$$

with p and ρ nondimensionalized to total conditions. Similiarly, the partial derivatives f_{1_θ} and f_{2_θ} are found to be:

$$f_{1_\theta} = \frac{-r\, \rho v^2 \left[\sin(\phi - \theta) \sin \theta + \cos(\phi - \theta) \cos \theta\right]}{\sin \phi} \tag{25}$$

$$f_{2_\theta} = - \frac{\rho v^2 \cos(\phi - \theta)}{\sin \phi} r \, . \tag{26}$$

Substituting Eqs. (23) to (26) into Eq. (16) and rearranging yields:

$$\left[- \frac{p}{M} + \frac{2\rho \sin(\phi - \theta) \cos \theta}{M\left(1 + \frac{\gamma - 1}{2} M^2\right) \sin \phi} - \frac{Mp \sin(\phi - \theta) \cos \theta}{\sin \phi} \right] \cos(\phi - \theta)$$

$$= \frac{\sin(\phi - \theta)}{\sin \theta} \left[\frac{\rho}{M\left(1 + \frac{\gamma - 1}{2} M^2\right)} - Mp \right]$$

$$\times \left[\sin(\phi - \theta) \sin \theta + \cos(\phi - \theta) \cos \theta\right]$$

or

$$-p\left(1+\frac{\gamma-1}{2}M^2\right)\cos(\phi-\theta)\sin\phi+2\rho\sin(\phi-\theta)\cos\theta\cos(\phi-\theta)$$

$$=\rho\sin^2(\phi-\theta)+\rho\sin(\phi-\theta)\cos(\phi-\theta)\cos\theta$$

$$-Mp\sin^2(\phi-\theta)\sin\theta M\left(1+\frac{\gamma-1}{2}M^2\right).$$

Combining Eqs. (17) and (18) results in the following expression for density

$$\rho^*=p\left(1+\frac{\gamma-1}{2}M^2\right).$$

This is then substituted into the relation above and the result is rearranged to give:

$$M^2=\frac{1}{\sin^2(\phi-\theta)\sin\theta}\left[\cos(\phi-\theta)-\sin(\phi-\theta)\cos\theta\cos(\phi-\theta)\right.$$

$$\left.+\sin^2(\phi-\theta)\sin\theta\right].$$

Utilizing the following trigonometric identities in this relation

$$\sin(\alpha\pm\beta)=\sin\alpha\cos\beta\pm\cos\alpha\sin\beta \tag{27}$$

$$\cos(\alpha\pm\beta)=\cos\alpha\cos\beta\pm\sin\alpha\sin\beta \tag{28}$$

and solving yields

$$M^2=\frac{1}{\sin^2(\phi-\theta)}.$$

This can be expressed in terms of the Mach angle as follows

$$\frac{1}{M}=\sin(\phi-\theta)=\sin\mu, \tag{29}$$

and hence

$$\phi=\theta+\mu. \tag{30}$$

This shows that the control surface is a left-running characteristic and Eq. (30) implies that

$$\frac{dr}{dz} = \tan(\theta + \mu) \quad \text{along} \quad DE. \tag{31}$$

By Eq. (13)

$$\lambda_2 = \frac{-f_{1_\theta}}{f_{2_\theta}}. \tag{32}$$

Introducing Eq. (30) into Eqs. (25) and (26) and applying the trigonometric identities gives:

$$f_{1_\theta} = -\frac{r\,\rho v^2 \cos(\theta - \mu)}{\sin\phi}$$

$$f_{2_\theta} = \frac{r\,\rho v \cos\mu}{\sin\phi}.$$

Substituting these relations into Eq. (32) and solving for λ_2 gives

$$\lambda_2 = \frac{-v\cos(\theta - \mu)}{\cos\mu}. \tag{33}$$

Equation (14) can now be solved for λ_3

$$\lambda_3 = \frac{-f_{1_\phi} + \lambda_2 f_{2_\phi}}{f_{3_\phi}}. \tag{34}$$

The partial derivatives f_{1_ϕ}, f_{2_ϕ} and f_{3_ϕ} can readily be written as:

$$f_{1_\theta} = \frac{\rho v^2 r \cos\theta \sin\theta}{\sin^2\phi} \tag{35}$$

$$f_{2_\phi} = \rho v r \frac{\sin\theta}{\sin^2\phi} \tag{36}$$

$$f_{3_\phi} = \frac{-1}{\sin^2\phi} . \tag{37}$$

Substituting Eqs. (35) to (37) and (33) into (34) yields:

$$\lambda_3 = \rho v^2 r \cos\theta \sin\theta - \frac{v \cos(\theta - \mu)}{\cos\mu} \rho v r \sin\theta$$

or

$$\lambda_3 = \rho v^2 r \sin\theta \left[\frac{\cos\theta \cos\mu - \cos(\theta - \mu)}{\cos\mu}\right]. \tag{38}$$

Employing the trigonometric identity brings

$$\lambda_3 = -\rho v^2 r \sin^2\theta \tan\mu. \tag{38}$$

Equations (30), (33), and (38) now yield the appropriate conditions to calculate the control surface. The constants λ_2 and λ_3 can be evaluated from the properties at point D. According to Eqs. (30) the control surface must coincide with a left-running characteristic. If this equation is satisfied, then it follows that the compatibility equation for a left-running characteristic must also be satisfied along the control surface, line DE. The compatibility equation for axisymmetric, isentropic, irrotational flow as found in Shapiro (1953) is

$$d\theta - \frac{\sqrt{M^2 - 1}}{M\left(1 + \frac{\gamma - 1}{2} M^2\right)} dM + \frac{\sin\mu \sin\theta}{r \sin(\theta + \mu)} dr = 0. \tag{39}$$

It can be shown that Eq. (39) is satisfied by Eqs. (33) and (38).

In order for the nozzle to be optimum for a fixed length constraint, the condition in Eq. (15) must be satisfied at point E. Utilizing Eqs. (8) to (10), (33), and (38), Eq. (15) becomes:

$$\left[(p - p_a) + \rho v^2 \frac{\sin\mu \cos\theta}{\sin(\theta + \mu)} r\right] - \frac{v \cos(\theta + \mu)}{\cos\mu} \rho v \frac{\sin\mu}{\sin(\theta + \mu)} r$$

$$- r\rho v^2 \sin^2\theta \tan\mu \cot(\theta + \mu) = 0,$$

which is the same as

$$\frac{p - p_a}{\frac{1}{2}\rho v^2 \tan\mu} = \frac{-2 \cos\mu \cos\theta}{\sin(\theta + \mu)} + \frac{2 \cos(\theta + \mu)}{\sin(\theta + \mu)} - 2 \sin^2\theta \cot(\theta + \mu).$$

The right-hand side of this equation may now be reduced by use of trigonometric identities. The final result is

$$\sin 2\theta = \frac{p - p_a}{\frac{1}{2}\rho v^2 \tan\mu} \quad ; \text{ at point E.} \tag{40}$$

Equations (33) and (38) for λ_2 and λ_3 are used in conjunction with the characteristic equations to define the flowfield and which relate the variables r, z, M, and θ are:

$$d\theta = \frac{\sqrt{M^2 - 1}}{M\left(1 + \frac{\gamma - 1}{2} M^2\right)} dM - \frac{1}{r\left(\sqrt{M^2 - 1} \cot\theta - 1\right)} dz \tag{41}$$

$$dr = \tan(\theta + \mu)\, dz \tag{42}$$

along a left-running characteristic and

$$d\theta = \frac{\sqrt{M^2 - 1}}{M\left(1 + \frac{\gamma - 1}{2} M^2\right)} dM + \frac{1}{r\left(\sqrt{M^2 - 1} \cot\theta - 1\right)} dz \tag{43}$$

$$dr = \tan(\theta - \mu)\, dz \tag{44}$$

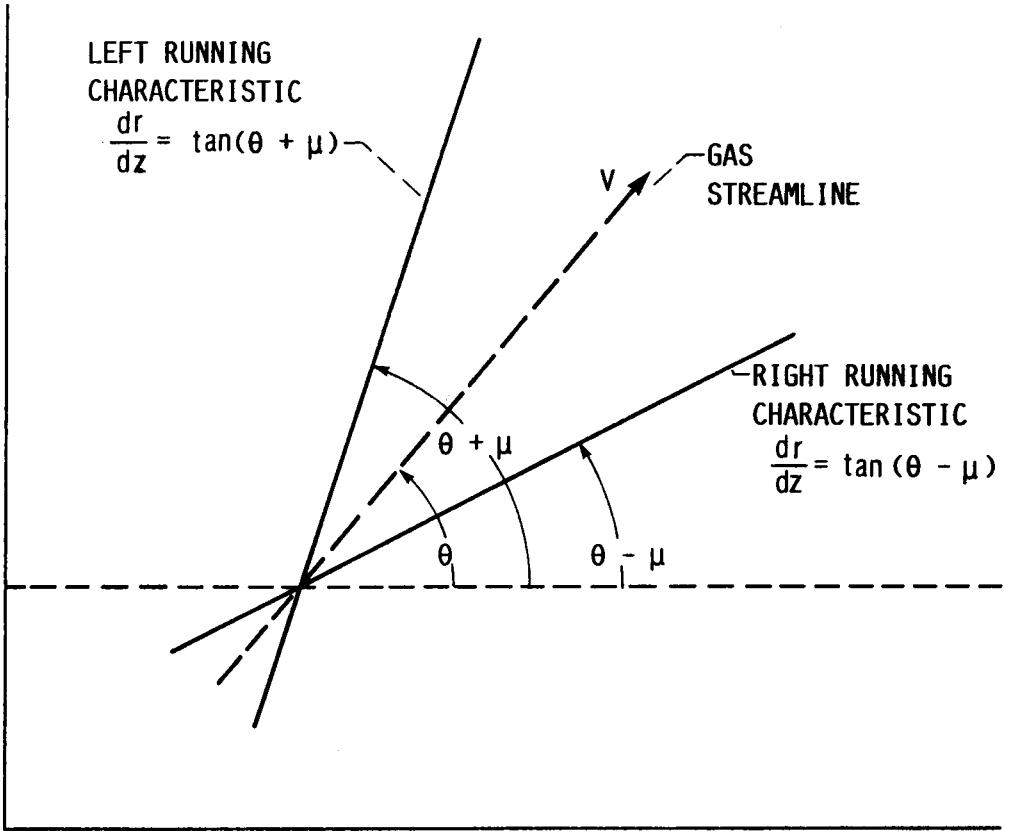

FIG. 6. - CHARACTERISTIC PLOT FOR TWO-DIMENSIONAL SUPERSONIC IRROTATIONAL FLOW

along a right-running characteristic, where the Mach angle μ is defined by:

$$\mu = \sin^{-1}\left(\frac{1}{M}\right). \tag{45}$$

The equations developed above are schematically shown in Fig. 6.

For two-dimensional Cartesian geometries Eq. (38) is independent of r and becomes

$$\lambda_3 = -\rho v^2 \sin^2\theta \tan \mu. \tag{46}$$

Equations (30) and (33) remain the same as for axisymmetric flow and along with Eq. (46) provide two equations in the two unknowns M and θ and hence yield a constant M and θ along the last characteristic. The character of flow is therefore that of a simple wave and this is in agreement with flow in the turning section of a two-dimensional Cartesian geometry nozzle.

Scarfed Truncation Point Computation

A schematic of the nomenclature used in the scarfed computer subroutine for computing the flow properties at a truncation point on the nozzle cowl are shown in Fig. 7. Truncation of the nozzle to point F allows the external flow to affect the mechanics of the solution. Since the nozzle is assumed to be underexpanded, i.e., the internal static pressure is greater than the ambient static pressure, a Prandtl-Meyer expansion fan and an oblique shock wave emanate from point F. Since the flow properties will differ in regions 2 and 2' in

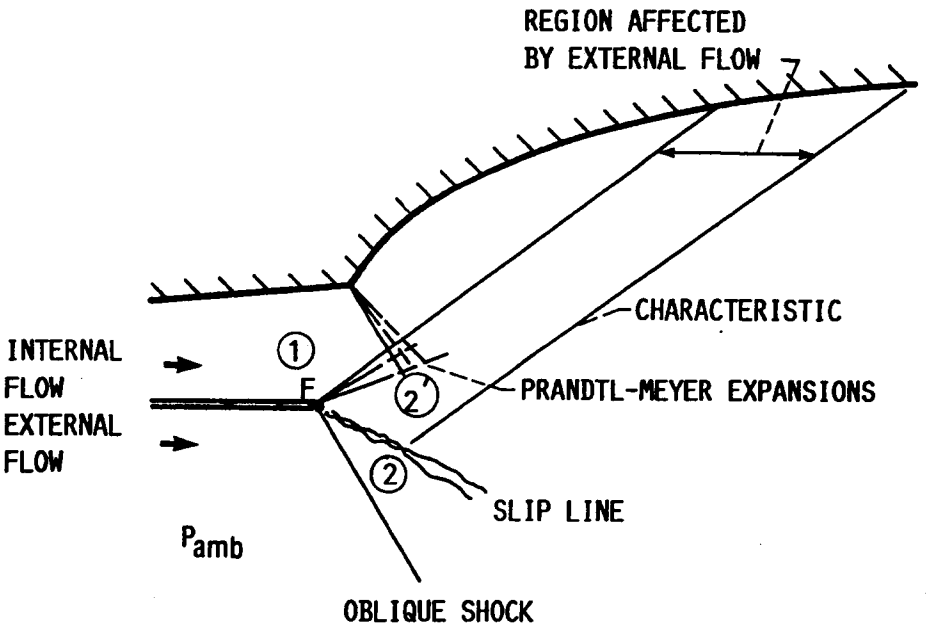

FIG. 7. - SCHEMATIC OF THE NOMENCLATURE USED IN SCARFED TRUNCATION POINT SUBROUTINE

Fig. 7, a slip line also forms at point F from the expansion of the internal flow. These flow phenomena are incorporated into the optimum nozzle program.

Figure 8 is a computer flow diagram of the scarfed subroutine. This subroutine computes the phenomena which occur at the cowl truncation point. Data is input for the ambient and nozzle Mach numbers M_a and M_1 respectively, specific heat ratios and static pressures. A check is performed on the ambient Mach number to determine whether its value is greater than 1.0. If M_a is supersonic, the static pressure behind the Prandtl-Meyer expansion is initialized by setting it equal to the ambient static pressure. If M_a is subsonic, the static pressure behind the Prandtl-Meyer expansion is initialized by computing the average of the ambient and nozzle static pressures. The flow regions computed by the scarfed subroutine are numbered as shown in Fig. 7.

Total pressures for the ambient flow and flow regions 1 and 2 along with the Prandtl-Meyer expansion angle ν, at state 1 are now computed from the isentropic flow equations developed in standard compressible flow texts, e.g. see John (1969) or Shapiro (1953). These relations are:

$$\frac{P_T}{p} = \left[1 + \frac{\gamma - 1}{2} M^2\right]^{\gamma/\gamma-1} \tag{47}$$

and

$$\nu = \sqrt{\frac{\gamma + 1}{\gamma - 1}} \tan^{-1} \sqrt{\frac{\gamma - 1}{\gamma + 1} (M^2 - 1)} - \tan^{-1} \sqrt{M^2 - 1} \cdot \tag{48}$$

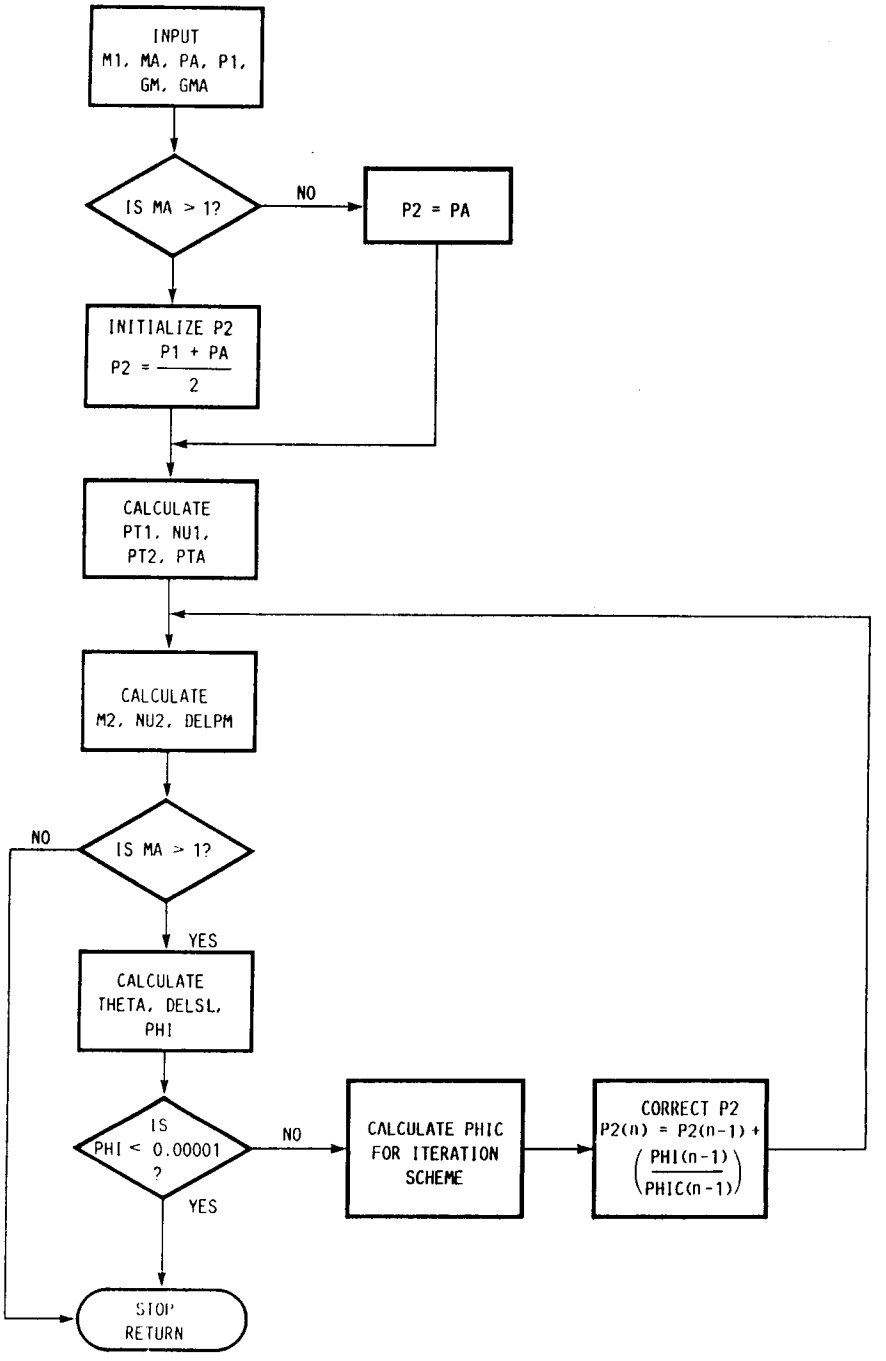

FIG. 8. - COMPUTER FLOW DIAGRAM FOR THE SCARFED TRUNCATION POINT SUBROUTINE

The total pressure at state 2 is set equal to the total pressure at state 2', because the total pressure across the slip line is constant. The Mach number at state 2 is next computed from Eq. (47) along with the corresponding Prandtl-Meyer expansion angle. The total Prandtl-Meyer expansion angle is then computed by calculating the absolute value of the difference in expansion angles at states 1 and 2.

The next step in the scarfed subroutine is to perform a test on the ambient Mach number to establish its value. For ambient Mach numbers less than 1.0, the subroutine returns to the main Rao program. For ambient Mach numbers greater than 1.0, the slip line angle, δ, and oblique shock wave angle, θ, are computed. The slip line angle is computed from

$$\cot \delta = = \tan \theta \left[\frac{(\gamma - 1)M_1^2}{2\left(M_1^2 \sin^2\theta - 1\right)} - 1 \right] \tag{49}$$

and the oblique shock wave angle from

$$\frac{P_2}{P_1} = \frac{2\gamma M_1^2 \sin^2\theta - (\gamma - 1)}{\gamma + 1} . \tag{50}$$

Both expressions are developed in the Ames Tables (1953).

The absolute value of the difference of the total Prandtl-Meyer expansion angle and the oblique shock wave angle, phi, is computed and checked for convergence. A difference of 0.00001 between successive passes was used as the convergence criteria in this study. If the convergence test fails, the subroutine computes the derivatives of

Eqs. (47) to (50) and these are used in Newton's method for iterative solution of simultaneous equations as developed in Press et al. (1986). Newton's method consists of computing the difference of the initial guesses and the derivatives of functions which define the guesses. The derivatives are assembled in a 2-by-2 matrix which appears as:

$$\begin{vmatrix} \frac{d\nu}{dM} & \frac{d\delta}{d\theta} \\ \frac{dp_2}{dM_2} & \frac{dp_2}{d\theta} \end{vmatrix}.$$

The derivatives in the matrix above are defined as:

$$\frac{dp_2}{dM_2} = \gamma\left(\frac{\gamma - 1}{\gamma + 1}\right) \frac{M_2 p_2}{\left(1 + \frac{\gamma - 1}{2} M_2^2\right)}$$

$$\frac{d\nu}{dM} = \frac{-1}{M_2 \sqrt{M_2^2 - 1}\left(1 + \frac{\gamma - 1}{2} M_2^2\right)}$$

$$\frac{d\delta}{d\theta} = \frac{\sin\delta \cos\delta}{p_a} \left\{ \frac{1}{(\xi - 1)} + \frac{1}{\left(\gamma M_1^2 - \xi - 1\right)} - \frac{\gamma + 1}{2}\left[2\gamma M_1^2 - (\gamma - 1) - (\gamma + 1)\xi\right]^{-1} - \frac{\gamma + 1}{2}\left[(\gamma + 1)\xi + (\gamma - 1)\right]^{-1} \right\}$$

(Note in the above $\xi = p_2/p_a$.)

$$\frac{dp_2}{d\theta} = \frac{4\gamma_a M_a^2 p_a \sin\theta \cos\theta}{\gamma_a + 1} .$$

This square matrix can be solved by the determinant method. The value of the determinant, phic, is based upon the values of the flow quantities computed for each iteration. The difference in total Prandtl-Meyer expansion angle and oblique shock wave angle, phi is now divided by phic and this value is then used to correct the initial guess of the state 2 static pressure. This is expressed in equation form as follows

$$p_{2_n} = p_{2_{n-1}} + \left(\frac{Phi}{Phic}\right)_{n-1} , \quad n = 1,2,\ldots,n.$$

The computational procedure outlined is now repeated until convergence is realized. The oblique shock wave angle, state 2 Mach number and static pressure are then used in the Rao program for constructing the right-running characteristic at the truncation point. The computer listing of this subroutine is contained in Appendix C.

Slip Line and Oblique Shock Wave Computation

The oblique shock wave and slip line that occur at the cowl truncation point may be curved or straight dependent upon the pressure difference between the ambient and nozzle flowfields. In general, the oblique shock wave and slip line will be curved because of the additional expansion which takes place in the internal nozzle flowfield. If the oblique shock wave is curved, the strength of the

shock will vary from point to point. The flow downstream of the shock is only isentropic along streamlines and is rotational because of gradients in the entropy and stagnation properties normal to the streamlines. For isentropic flows, the entropy is constant along streamlines.

Zucrow and Hoffman (1977) develop the governing equations for steady adiabatic flow of an inviscid compressible fluid, which are used to derive the characteristic equations for a rotational isentropic flow. The continuity, momentum, and speed of sound (used in place of energy), equations are:

$$\nabla \bullet (\rho \vec{v}) = 0 \tag{51}$$

$$\rho \frac{D\vec{v}}{Dt} + \nabla p = 0 \tag{52}$$

$$\frac{Dp}{Dt} - a^2 \frac{D\rho}{Dt} = 0. \tag{53}$$

Expressing Eqs. (51) to (53) in Cartesian coordinates for two-dimensional flow yields:

$$\rho u_x + \rho v_y + u\rho_x + v\rho_y + \frac{\delta \rho v}{y} = 0 \tag{54}$$

$$\rho u u_x + \rho v u_y + p_x = 0 \tag{55}$$

$$\rho u v_x + \rho v v_y + p_y = 0 \tag{56}$$

$$up_x + vp_y - a^2 u\rho_x - a^2 v\rho_y = 0 \tag{57}$$

where $\delta = 0$ for planar flow, and $\delta = 1$ for axisymmetric flow.

The characteristic and compatibility equations which result from Eqs. (54) to (57) for a two-dimensional isentropic rotational supersonic flow developed in Zucrow and Hoffman (1977) are:

(a) Characteristic Equations

$$\left(\frac{dy}{dx}\right)_o = \lambda_o = \frac{v}{u} \qquad \text{(streamline)} \qquad (58)$$

$$\left(\frac{dy}{dx}\right)_\pm = \lambda_\pm = \tan(\theta \pm \mu) \qquad \text{(Mach lines)} \qquad (59)$$

(b) Compatibility Equations

$$\rho v\, dv + dp = 0 \qquad \text{(along streamlines)} \qquad (60)$$

$$dp - a^2 d\rho = 0 \qquad \text{(along streamlines)} \qquad (61)$$

$$\frac{\sqrt{M^2 - 1}}{\rho v^2} dp_\pm d\theta + \delta \left[\frac{\sin\theta\, dx_\pm}{yM\cos(\theta \pm \mu)}\right] = 0 \qquad \text{(along Mach lines).} \qquad (62)$$

Figure 9 shows a plot of the characteristics for steady two-dimensional supersonic rotational flow. The characteristic and compatibility equations derived for the Mach lines remain the same as those equations derived for irrotational flow. However, two additional equations are obtained. These are the streamlines (counted twice) and the compatibility relations along the streamlines. The compatibility equations are the Bernoulli equation and the speed of sound relation.

The finite difference equations derived by Zucrow and Hoffman for two-dimensional steady isentropic rotational flow equations are:

$$\Delta y_o = \lambda_o \Delta x_o \qquad (63)$$

$$R_o \Delta v_o + \Delta p_o = 0 \qquad (64)$$

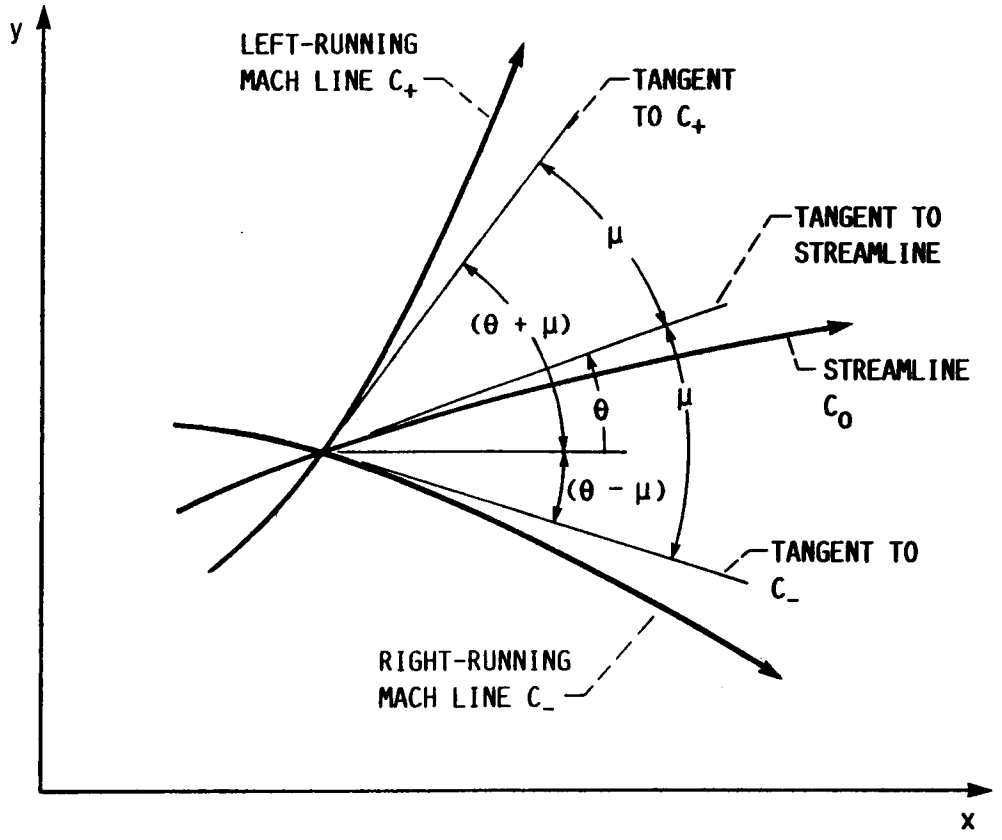

FIG. 9. - CHARACTERISTIC PLOT FOR STEADY TWO-DIMENSIONAL SUPERSONIC ROTATIONAL FLOW

$$\Delta p_o - A_o \Delta \rho_o = 0 \tag{65}$$

$$\Delta y_\pm = \lambda_\pm \Delta x_\pm \tag{66}$$

$$Q_\pm \Delta p \pm \Delta \theta_\pm + S_\pm \Delta x_\pm = 0 \tag{67}$$

$$A_o = a^2 \tag{68}$$

$$Q = \frac{\sqrt{M^2 - 1}}{\rho v^2} \tag{69}$$

$$R_o = \rho v \tag{70}$$

$$S = \frac{\delta \sin \theta}{yM \cos(\theta \pm \mu)} \tag{71}$$

where C_- denotes a right-running characteristic, C_+ denotes a left-running characteristic and C_o denotes a streamline as shown in Fig. 9.

The numerical algorithms for applying Eqs. (63) to (71) are based upon a modified Euler predictor-corrector method. In the predictor step, each of the coefficients in the finite difference equations are calculated at the known initial points. In the corrector step, average values of the four primary dependent variables v, θ, p, and ρ are computed along each three of the characteristics, and the coefficients of the finite difference are calculated by employing those average properties. This numerical integration algorithm is termed an average property method.

The steady two-dimensional supersonic rotational flow equations derived above have to be incorporated into the Rao computer program to

complete the construction of the flowfield between the external oblique shock wave and the slip line. Figure 10 provides an indication of the changes incorporated into the Rao computer program. The top portion, Fig. 10(a), shows left and right-running characteristics emanating from the nozzle cowl. The bottom portion, Fig. 10(b) is a schematic of the mesh used to calculate the rotational flow. The truncation point on the nozzle cowl corresponds to grid point 11 on the mesh. The flow conditions at this grid point were calculated by the scarfed routine discussed previously.

The flow properties at grid point 21 are computed by assuming that the flow properties at this point are defined by right-running flow characteristics from the internal flow (which is discussed below) with an assumed Mach number. The program then iterates using the continuity relation between the left-running characteristic from point A to point 11 and the right-running characteristic from point A to point 21 to establish the final value of the conditions at point 21. Once the flow properties are determined at grid point 21, the properties at grid points 11 and 21 are used to find the flow properties at grid point 23 using the oblique shock wave relations and the method of characteristics for rotational isentropic flow. The conditions at points 21 and 23 are then iterated upon until convergence is realized in the pressure loss across the oblique shock wave. The flow properties at grid point 22 are computed by taking an average of the properties at grid points 21 and 23. The flow properties at following mesh points are subsequently computed.

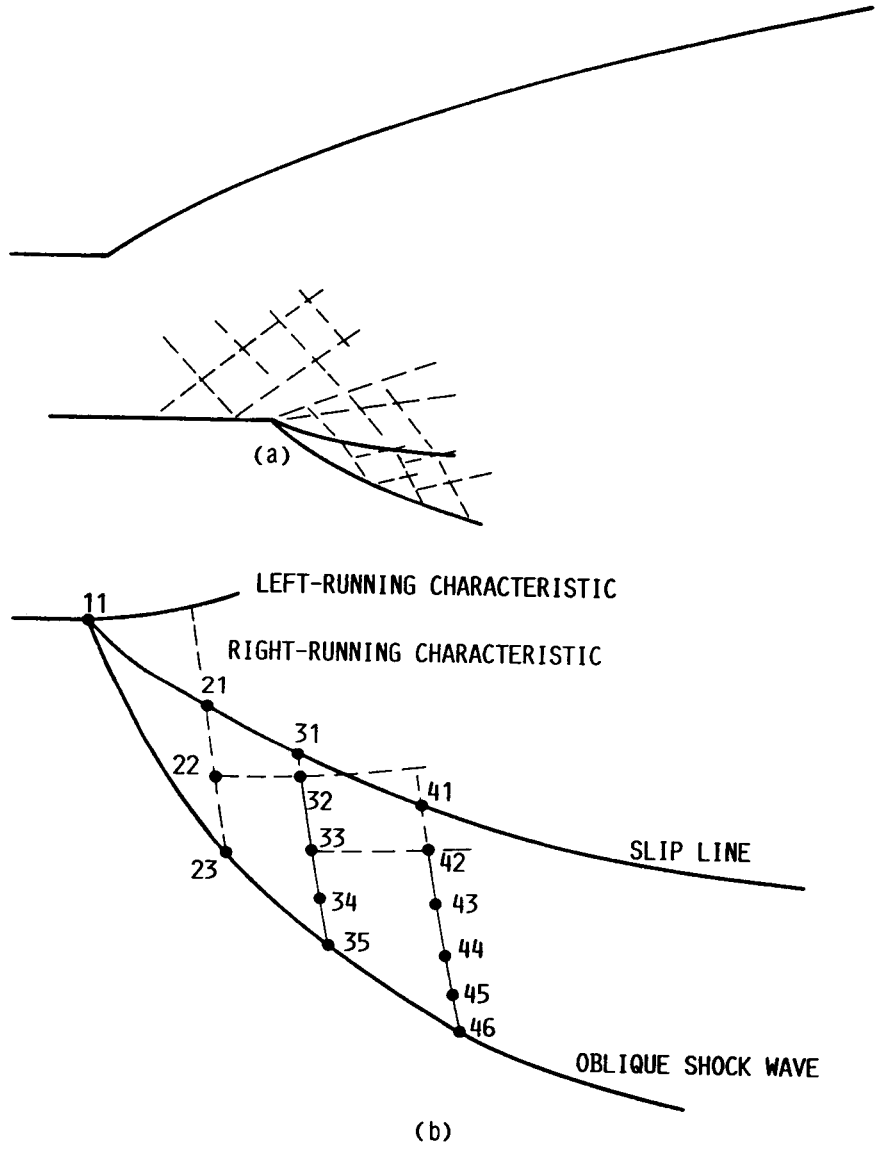

FIG. 10. - SCHEMATIC OF ROTATIONAL FLOW MODIFICATIONS INCORPORATED INTO THE RAO PROGRAM

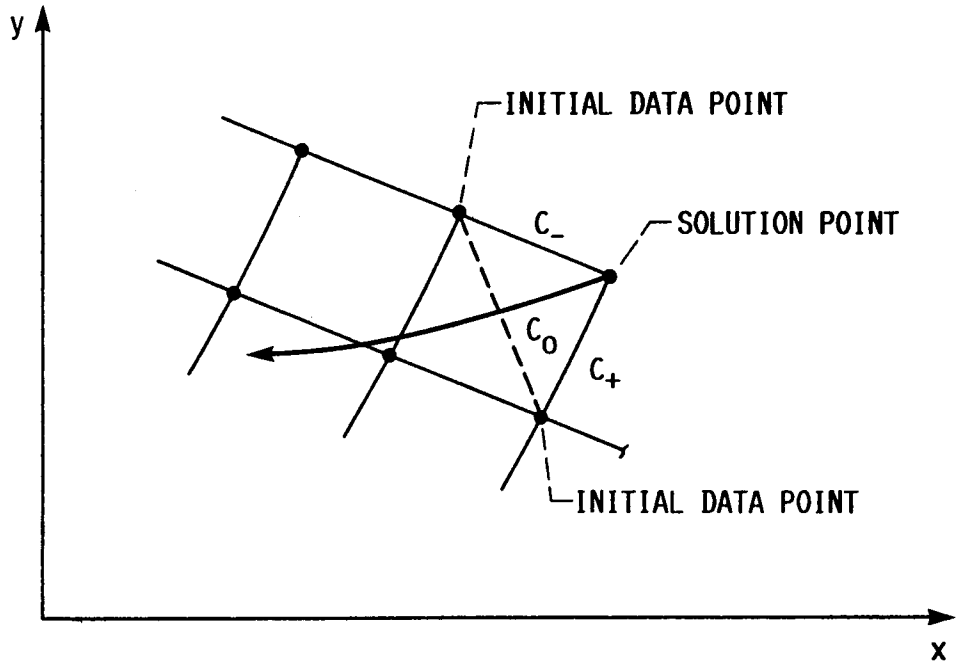

FIG. 11. - FINITE DIFFERENCE NETWORK FOR TWO-DIMENSIONAL SUPERSONIC ROTATIONAL FLOW

Interior Point Computation

As the calculation proceeds, a numerical algorithm is required for calculation of an interior point. The finite difference network used in this analysis is illustrated in Fig. 11. Figure 12 is a schematic of the unit process for determining an interior point. Points 1 and 2 are initial-data points on the C_- and C_+ Mach lines and line 12 connects these points. The rearward running streamline C_0 intersects line 12 at point 3 and the properties at point 3 are computed by linear interpolation.

The following four equations are obtained by writing Eqs. (63) and (66) in finite difference form in terms of points 1, 2, 3, and 4, and from the equation of the diagonal line 12.

$$y_3 - \lambda_0 x_3 = y_4 - \lambda_0 x_4 \tag{72}$$

$$y_4 - \lambda_+ x_4 = y_2 - \lambda_+ x_2 \tag{73}$$

$$y_4 - \lambda_- x_4 = y_1 - \lambda_- x_1 \tag{74}$$

$$y_3 - \lambda_{12} x_3 = y_3 - \lambda_{12} x_2 \tag{75}$$

where λ_{12}, λ_+, λ_-, and λ_0, are the slopes of line 12, the left-running characteristic, the right-running characteristic, and the streamline, respectively. Equations (72) to (75) are solved simultaneously for x_3, y_3, x_4, and y_4. The quantities v, θ, p, and ρ are then calculated by linear interpolation as discussed above. The Euler predictors for an interior point are:

$$\lambda_+ = \tan(\theta_2 + \mu_2) \tag{76}$$

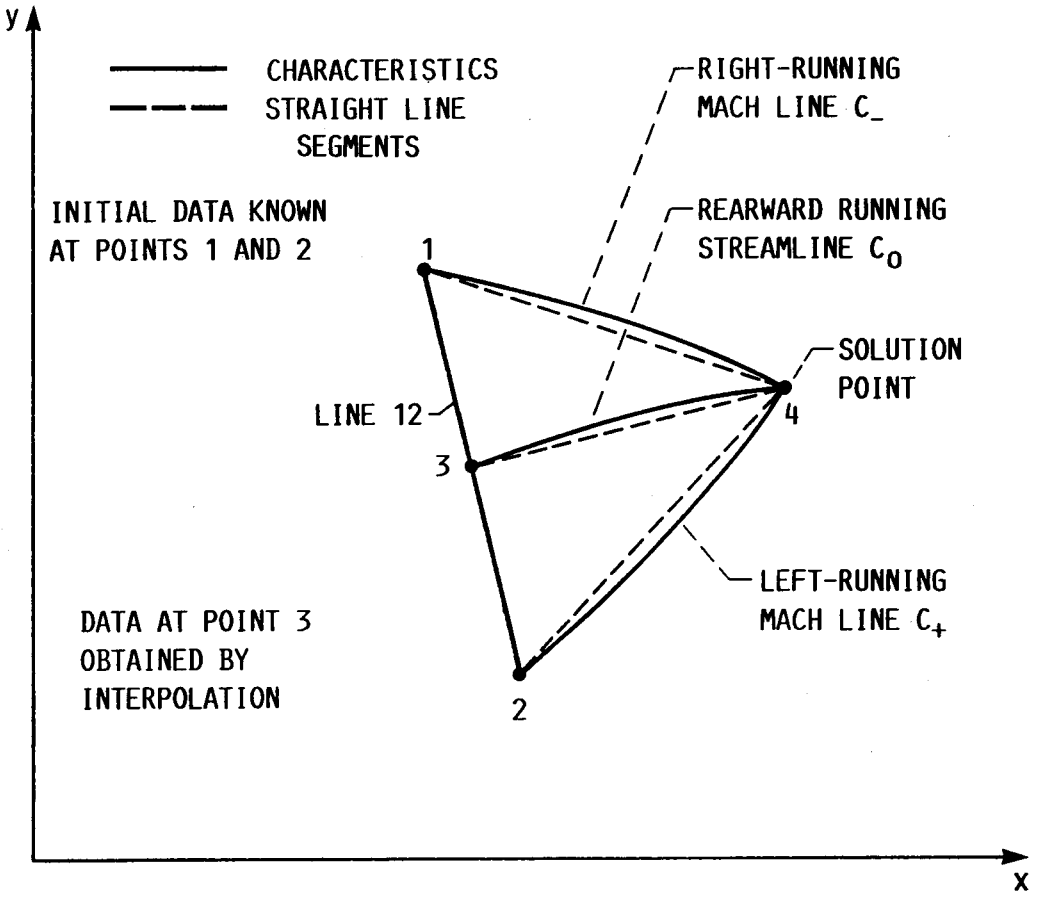

FIG. 12. - SCHEMATIC OF THE UNIT PROCESS FOR AN INTERIOR POINT COMPUTATION

$$\lambda_- = \tan(\theta_1 - \mu_1). \tag{77}$$

The value of λ_0 depends upon the flow angle at point 3, which is not known until point 3 is located and the corresponding flow properties have been calculated by linear interpolation. An iterative procedure must be employed for determining the location of point 3 during each pass through the modified Euler predictor-corrector algorithm. The initial estimate for θ_3 is obtained for the Euler predictor as follows:

$$\theta_3 = \frac{\theta_1 + \theta_2}{2} . \tag{78}$$

Equations (76) and (77) are then solved simultaneously for x_3 and y_3, and the corresponding θ_3 is found by linear interpolation. The procedure may then be repeated using the new value θ_3 to obtain improved values of x_3, y_3, and θ_3. The procedure is repeated until the change in the values of x_3 and y_3 diminish below the specified tolerance.

The compatibility equation, Eq. (67) which is valid along Mach lines, may be written in finite difference form as:

$$Q_+ p_4 + \theta_4 = T_+ \tag{79}$$

$$Q_- p_4 + \theta_4 = T_- , \tag{80}$$

where

$$T_+ = -S_+(x_4 - x_2) + Q_+ p_2 + \theta_2 \tag{81}$$

$$T_- = -S_-(x_4 - x_1) + Q_- p_1 - \theta_1 . \tag{82}$$

For the Euler predictor the following equations are derived:

$$Q_+ = \frac{\sqrt{M^2 - 1}}{\rho_2 v_2^2} \qquad S_+ = \frac{\delta \sin \theta_2}{y_2 M_2 \cos(\theta_2 + \mu_2)} \tag{83}$$

$$Q_- = \frac{\sqrt{M^2 - 1}}{\rho_1 v_1^2} \qquad S_- = \frac{\delta \sin \theta_1}{y_1 M_1 \cos(\theta_1 + \mu_1)} \tag{84}$$

These equations are now solved simultaneously for p_4 and θ_4.

Writing Eqs. (64) and (65), the compatibility equations valid along streamlines, in finite difference form gives

$$R_o v_4 + p_4 = R_o v_3 + p_3 = T_{o_1} \tag{85}$$

$$p_4 - A_o \rho_4 = p_3 - A_o \rho_3 = T_{o_2} \tag{86}$$

For the Euler predictor

$$R_o = \rho_3 v_3 \ , \ A_o = a_3^2 \tag{87}$$

where $a = a(p, \rho)$. Equations (85) and (86) are now solved for v_4 and p_4. This completes the application of the Euler predictor algorithm. The computational equations derived for steady two-dimensional isentropic rotational supersonic flow are summarized as follows:

$$y_3 - \lambda_o x_3 = y_4 - \lambda_o x_4 \tag{72}$$

$$y_4 - \lambda_+ x_4 = y_2 - \lambda_+ x_2 \tag{73}$$

$$y_4 - \lambda_- x_4 = y_1 - \lambda_- x_1 \tag{74}$$

$$y_3 - \lambda_{12} x_3 = y_2 - \lambda_{12} x_2 \tag{75}$$

$$Q_+ p_4 + \theta_4 = T_+ \tag{79}$$

$$Q_- p_4 - \theta_4 = T_- \tag{80}$$

$$R_o v_4 + p_4 = T_{o_1} \tag{85}$$

$$p_4 - A_o \rho_4 = T_{o_2} \tag{86}$$

Improved values for the location of and the corresponding flow properties at point 4 may be computed by repeating the steps outlined above for the Euler predictor algorithm, but employing average values of v, θ, p, and ρ along each characteristic. Hence,

$$\lambda_+ = \tan(\theta_+ + \mu_+) \tag{88}$$

where

$$p_+ = \frac{p_2 + p_4}{2}, \quad \theta_+ = \frac{\theta_2 + \theta_4}{2}, \quad v_+ = \frac{v_2 + v_4}{2}, \quad \rho_+ = \frac{\rho_2 + \rho_4}{2} \tag{89}$$

For a simple thermodynamic system

$$a = a(p, \rho) \tag{90}$$

and it follows

$$a_+ = a(p_+, \rho_+) \tag{91}$$

Then,

$$M_+ = \frac{v_+}{a_+}, \quad a_+ = \sin^{-1}\left(\frac{1}{M_+}\right). \tag{92}$$

The coefficients λ_-, λ_o, Q_+, Q_-, S_+, S_-, R_o, and A_o are determined in a similar manner.

The speed of sound, a, now has to be determined from Eq. (91). Assuming a perfect gas, Eq. (91) takes the form

$$a^2 = \frac{\gamma p}{\rho} \tag{93}$$

Correspondingly, the temperature T, is given by

$$T = T(p, \rho) \tag{94}$$

and for a perfect gas

$$T = \frac{p}{\rho R_g} \tag{95}$$

The pressure p and density ρ are used to calculate the temperature T, Mach number M, and the speed of sound a, in a separate subroutine. By calculating the fluid properties in this manner, the different unit processes can be determined by the method of characteristics, which are independent of the equations of state for the fluid.

Iteration and convergence are controlled on the axis of symmetry. The ratio $\sin \theta_2/y_2$ in the coefficient S is approximated by the ratio $\sin \theta_1/y_1$ for the predictor. For the corrector, that ratio is based upon average values of θ and y, which are nonzero.

External Shock Wave Point Computation

Figure 13 illustrates schematically the unit process for determining an external shock wave point. Properties are known at point 1 on the downstream side of the shock wave, and point 2 is a known point on the previous right-running Mach line 12. The free-stream flow properties M_∞, v_∞, p_∞, and ρ_∞ are also known. Point 4, on the downstream side of the shock wave, is the external shock wave point. This point is located at the intersection of the shock wave

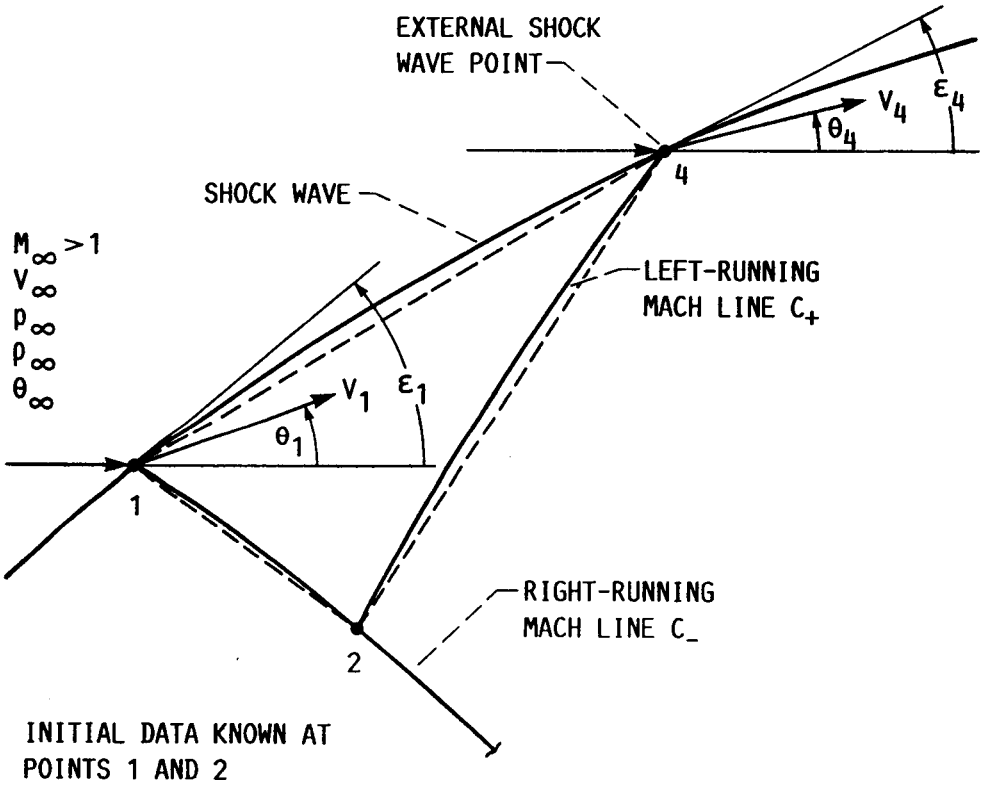

FIG. 13. - SCHEMATIC OF THE UNIT PROCESS FOR AN EXTERNAL SHOCK WAVE POINT COMPUTATION

from point 1 and the left-running Mach line 24. The slope of shock wave 14 is computed from the average value of the two wave angles ε_1 and ε_2 at the points 1 and 4, respectively. These wave angles are functions of the free-stream Mach number M_a and the flow turning angles θ_1 and θ_4.

To determine the location of, and the properties at point 4, an iterative procedure is employed. A value of the wave angle ε_4 is assumed at point 4. The finite difference equation for the shock wave 14 is

$$y_4 - y_1 = \lambda_s(x_4 - x_1) = \tan\left(\frac{\varepsilon_1 + \varepsilon_4}{2}\right)(x_4 - x_1) \tag{96}$$

and the equation of the left-running Mach line 24 is

$$y_4 - y_2 = \lambda_+(x_4 - x_2). \tag{97}$$

The location of point 4 is computed by solving Eqs. (96) and (97) simultaneously for x_4 and y_4. Equation (79), the single compatibility equation valid for left-running Mach lines, must also be satisfied for this computation.

Incorporation of Rotational Flow

The equations developed for the interior point and external shock wave point computation have to be incorporated into the Rao program. The flow diagram in Fig. 14 illustrates how this can be accomplished.

A point on the slip line is computed as previously described. A comparison is now performed to determine if the ambient static pressure

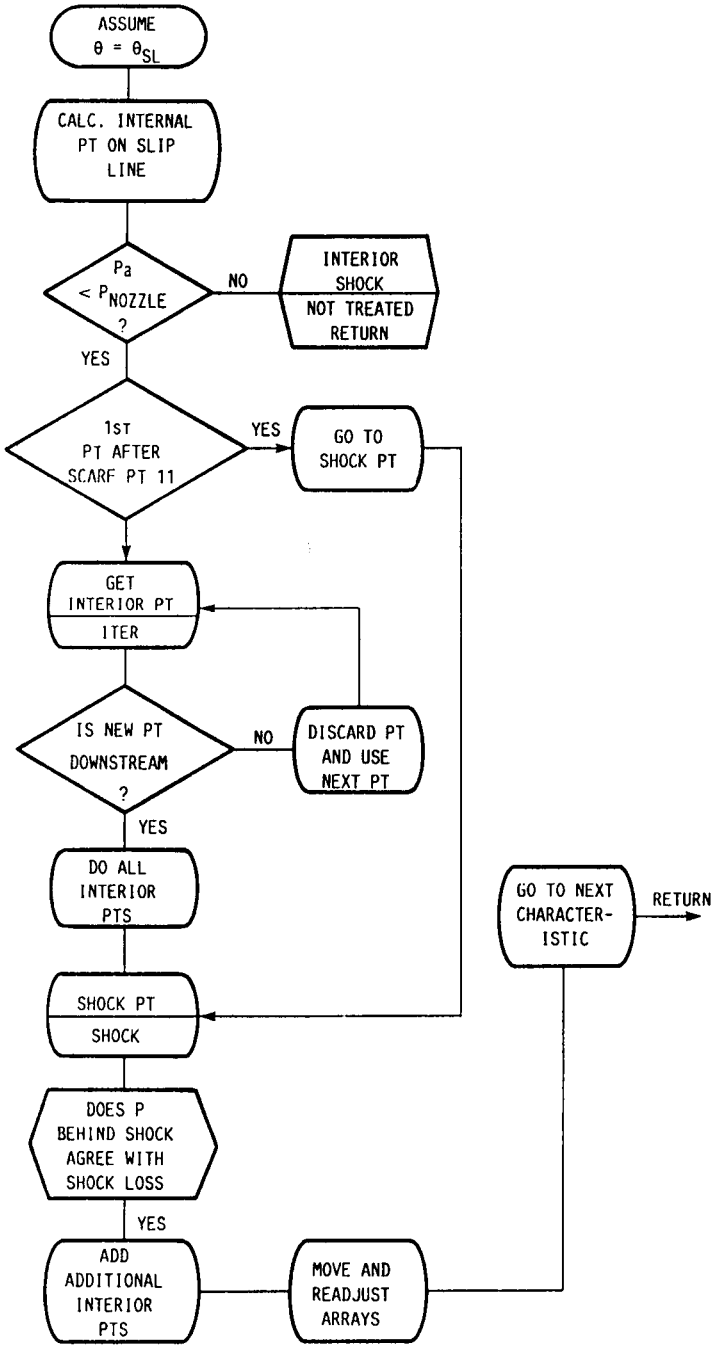

FIG. 14. - COMPUTER FLOW DIAGRAM FOR ROTATIONAL FLOW MODIFICATIONS

is less than the nozzle static pressure. If the ambient static pressure is greater than the nozzle static pressure, the subroutine returns to the main program (this case would depict a shock wave forming in the interior of the nozzle and this analysis will fail for this case). If the ambient static pressure is less than the nozzle static pressure, the computation continues.

Next, the interior point is examined to determine whether it is the first point after the scarfed truncation point. If it is the first point, the routine computes a shock point using the external shock wave point routine. A shock loss is then computed and compared to the pressure behind the shock wave. If this loss agrees with the pressure behind the shock wave additional interior points are considered. These points are moved and readjusted into arrays. The routine then advances to the next characteristic and the computation returns to the main program.

On the other hand, if the point computed on the slip line is not the first point after the scarfed truncation point, an interior point computation is performed. If this interior point is upstream of the first slip line point (see Fig. 10), this point is discarded and the next point is used. If this point is downstream of the scarfed truncation point, all interior points are calculated. A shock point is subsequently computed and the computation continues as described above. The computation of the kernel continues downstream until the contour is defined.

Seagull Analysis

The design of a truncated scarfed nozzle can be analyzed using a shock fitting method for two-dimensional supersonic flows. This shock fitting method referred to as Seagull, was developed by Salas (1976). Seagull can be used to analyze complex two-dimensional or axisymmetric supersonic inviscid flows of a perfect gas. Seagull is limited to analyzing flows whose axial component of Mach number remains supersonic (hyperbolic equations of motion are used in this analysis and for subsonic flows these equations become elliptic). This code can be used to compute flowfields produced by a single duct or several ducts that are merged. Jets and plumes can also be analyzed by Seagull. This code will be used in this thesis for a comparison with the results from the Rao method.

Flow Correlations

Manipulation of Eqs. (49) and (50) produces a functional relationship for the external and nozzle Mach numbers, oblique shock wave and slip line angles, ambient and nozzle static pressures, and dynamic pressure coefficient.

Rearranging Eqs. (49) and (50) yield the following relations:

$$\left(\frac{\gamma + 1}{4}\right)\left(\frac{p_2 - p_1}{q_1}\right) = \sin^2\theta + \frac{1}{\gamma M_a^2} \tag{98}$$

$$\tan \delta = \left[\frac{(p_2 - p_1)/q_1}{2 - (p_2 - p_1)/q_2}\right]. \tag{99}$$

These relations exhibit a mathematical relationship of a linear nature, i.e, having the form $y = mx + b$, and can be graphically presented. This can provide a simple graphical representation of the flow conditions at the truncated cowl lip point.

RESULTS AND DISCUSSION

Flow Correlations

Equations (99) and (100), the relations relating the slip line and oblique shock wave angles, ambient and nozzle static pressures, are plotted in Figs. 15 and 16.

Figure 15 is a plot of dynamic pressure coefficient times specific heat ratio versus oblique shock wave angle for constant values Mach number. Straight line curves result for this plot and this illustrates the linear nature of Eq. (99). For a given dynamic pressure coefficient, ambient specific heat ratio, and ambient Mach number, the oblique shock wave angle can be determined or for any of three previously mentioned flow parameters, a fourth can be determined.

A plot of oblique shock wave angle versus dynamic pressure coefficient for constant values of slip line angle is shown in Fig. 16. The curves in this plot were constructed for slip line angles of 1.0°, 2.0°, 10.0°, 25.0°, and 50.0°. These curves exhibit a hyperbolic behavior due to the cotangent trigonometric function in Eq. (100). As the slip line angle is increased the curves become progressively linear and tend towards infinity as the dynamic pressure coefficient is increased.

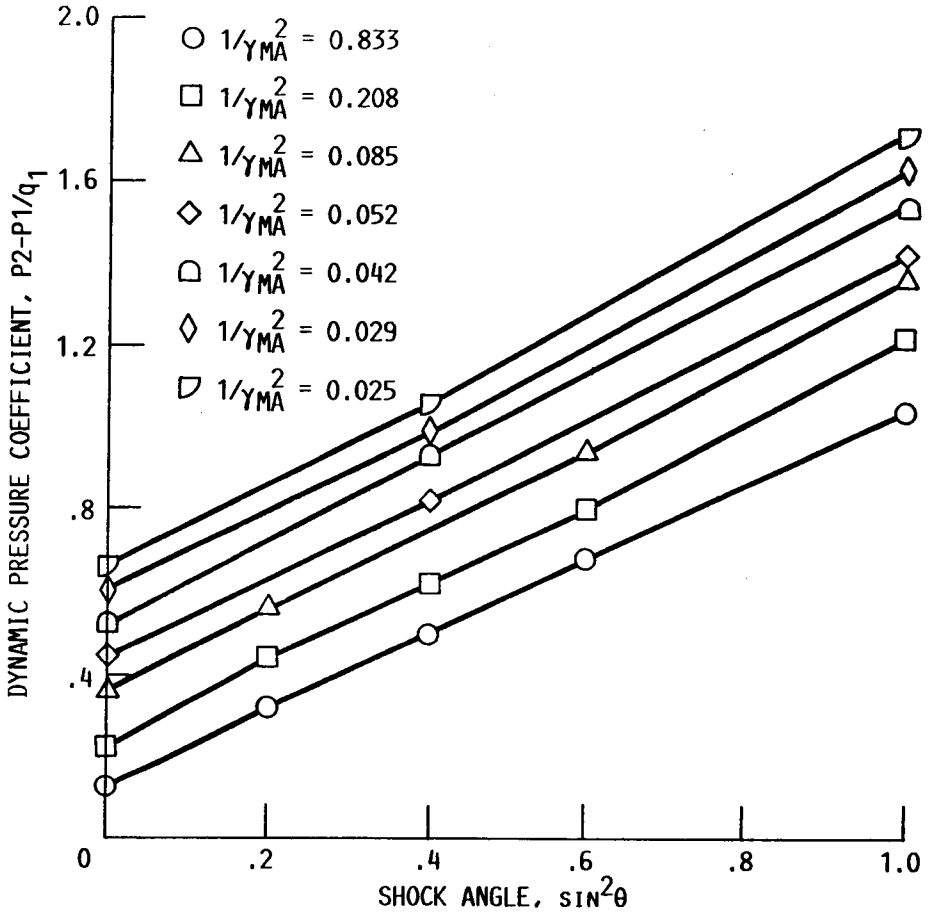

FIG. 15. - PLOT OF Sin^2 OF OBLIQUE SHOCK WAVE ANGLE VERSUS DYNAMIC PRESSURE COEFFICIENT

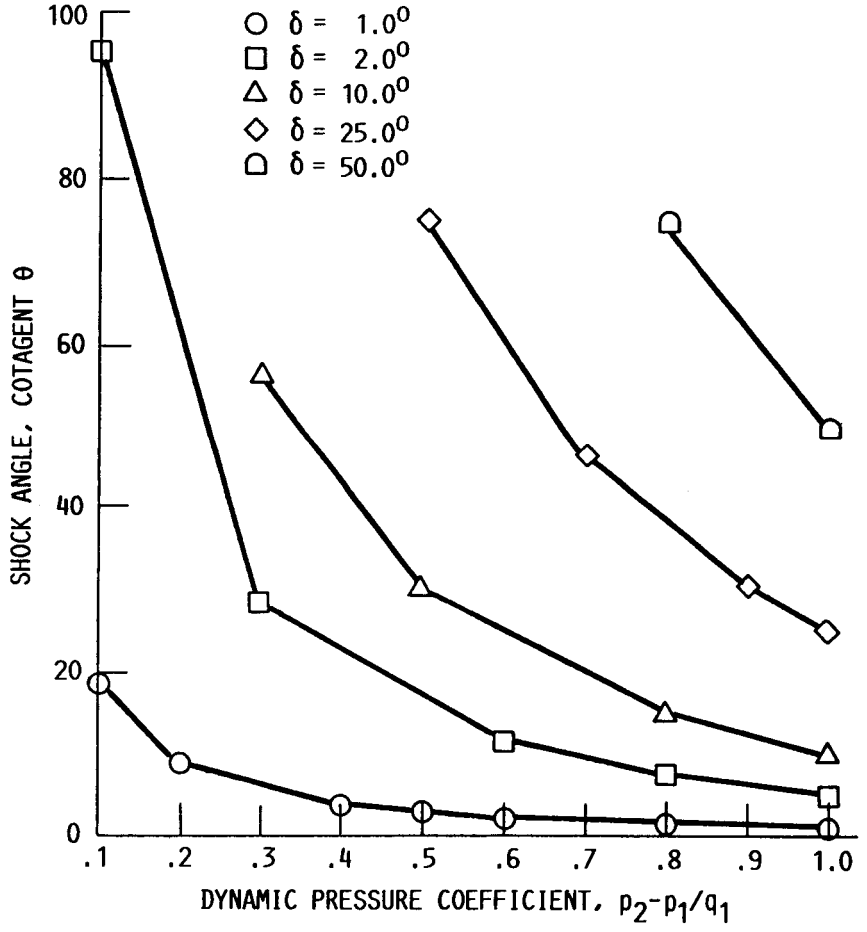

FIG. 16. - PLOT OF DYNAMIC PRESSURE COEFFICIENT VERSUS COTANGENT OF OBLIQUE SHOCK WAVE ANGLE

Truncated Scarfed Nozzle Computation

A truncated scarf nozzle was calculated for a design Mach number of 6.0, i.e, the Mach number at last nozzle characteristic is 6.0 with an external flow Mach number of number of 5.0, and external and internal specific heat ratios of 1.4. An area ratio of 90.0, nozzle ramp length of 300.0 inches, nozzle cowl length of 15.0 inches, nozzle throat Mach number of 1.24, nozzle throat temperature of 2500 °R, along with ambient static pressure of 0.150 psia and 100 psia for the nozzle throat total pressure complete the input used for this design. Pressures and coordinates computed in this analysis are nondimensionalized with respect to the nozzle throat conditions.

A nontruncated scarfed nozzle was also designed to compare the effect of truncation. The nontruncated nozzle was computed for the same design Mach number as the truncated nozzle (the external flow does not affect the nozzle computation, refer to Fig. 2). The nontruncated nozzle computation requires approximately 10 seconds of cpu time on an IBM 3033 mainframe computer, while the truncated scarfed case requires approximately 20 seconds of cpu time.

Figure 17 is a plot of nozzle cowl length versus nozzle thrust coefficient. The scarfed nozzle designed for a Mach number of 6.0 was selectively truncated for nozzle cowl lengths ranging from 50 inches to 12.5 inches. A nozzle thrust coefficient of 1.6661 is computed for the nontruncated case and is invariant with cowl truncation down to 20.0 inches. Truncating the cowl shorter than 20.0 inches will cause the nozzle thrust coefficient to drop sharply as shown in Fig. 17. A

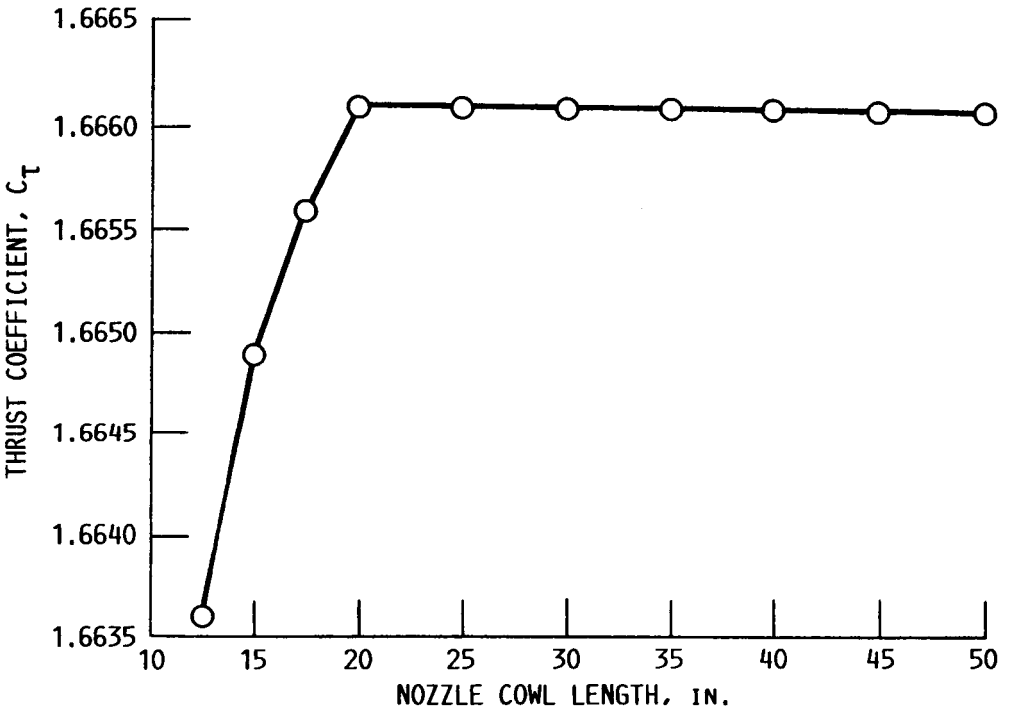

FIG. 17. - PLOT OF NOZZLE COWL LENGTH VERSUS NOZZLE THRUST COEFFICIENT

nozzle cowl length of 20.0 inches corresponds to point where the last nozzle ramp characteristic intersects the cowl surface as illustrated in Fig. 2.

The nontruncated nozzle and truncated scarfed nozzle were then analyzed with the Seagull code. These computations were performed on the Cray X-MP supercomputer and required approximately 30 seconds of cpu time per case.

Figures 18 to 22 are plots of flow path geometry, static pressure, axial velocity, axial Mach number, and Mach number contours for the nontruncated nozzle. Figures 19 and 20 display smooth distributions of static pressure and axial velocity plots, where the Mach number distribution in the plot of Fig. 21 shows a wave in the lower wall Mach number. The wave can be attributed to the Prandtl-Meyer expansion fan which occurs at the beginning of the turning section past the throat section and the intersection of the two families of characteristics. This slight compression wave is clearly shown in Fig. 22 in the Mach number contour plot.

The analysis of the truncated scarfed nozzle case are presented in Figs. 23 to 28. Figure 23 is a plot of the flow path geometry with the cowl truncated at 15.0 inches. The solid line extending past this point is a boundary drawn by the Seagull program. Figure 24 contains the static pressure plot of the truncated scarfed nozzle and shows an abrupt drop in the static pressure distribution on the lower wall at the truncation point. The lower wall static pressure becomes equal to the freestream static pressure slightly beyond the truncation point.

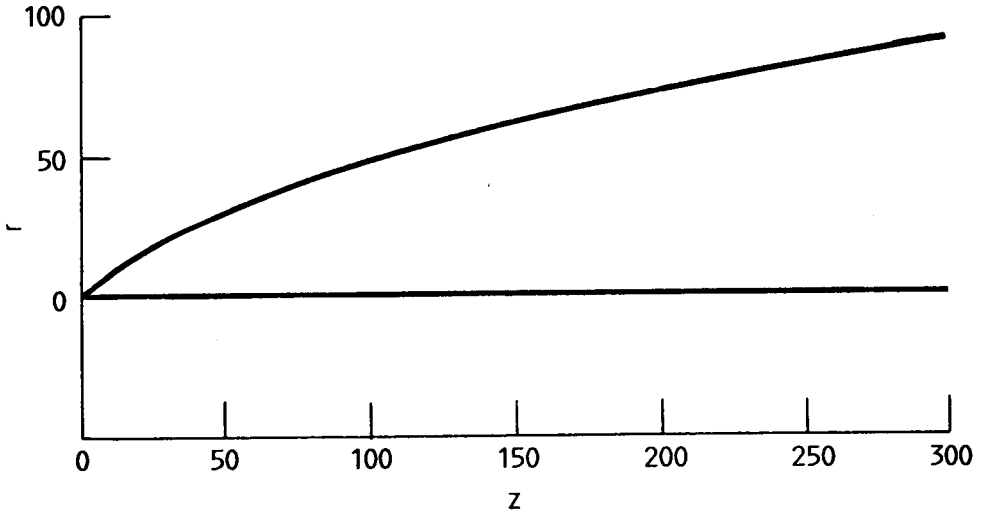

FIG. 18. - FLOW PATH GEOMETRY PLOT OF NONTRUNCATED NOZZLE

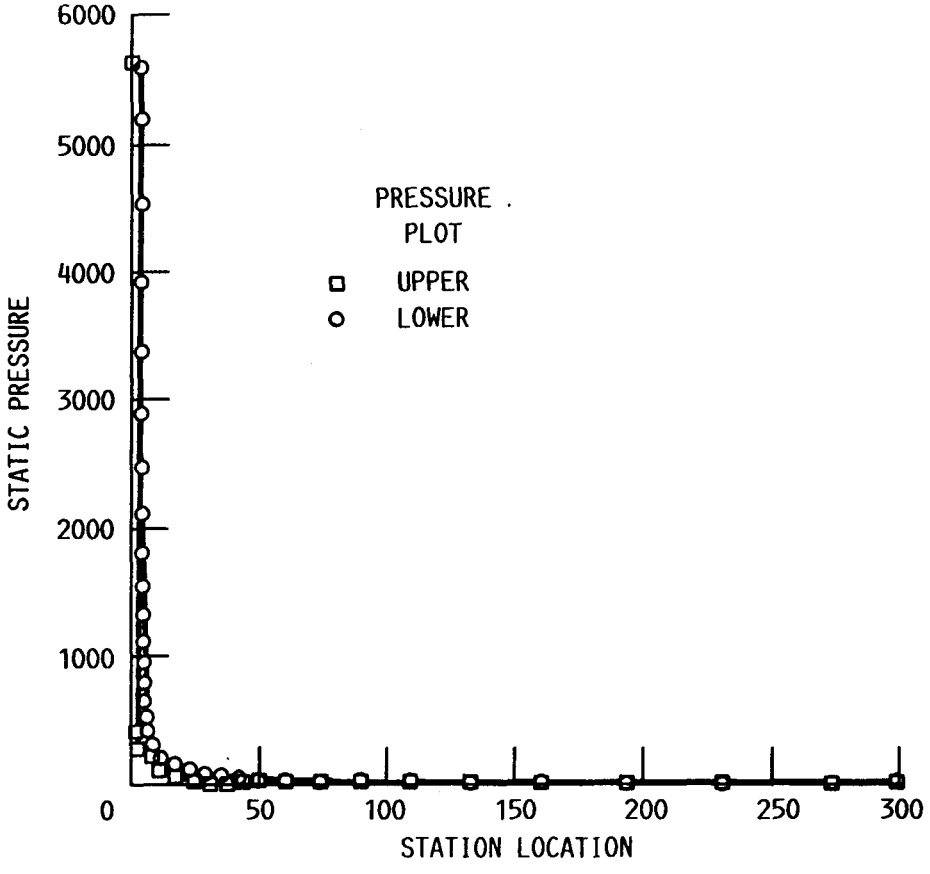

FIG. 19. - WALL STATIC PRESSURE PLOT OF NONTRUNCATED NOZZLE

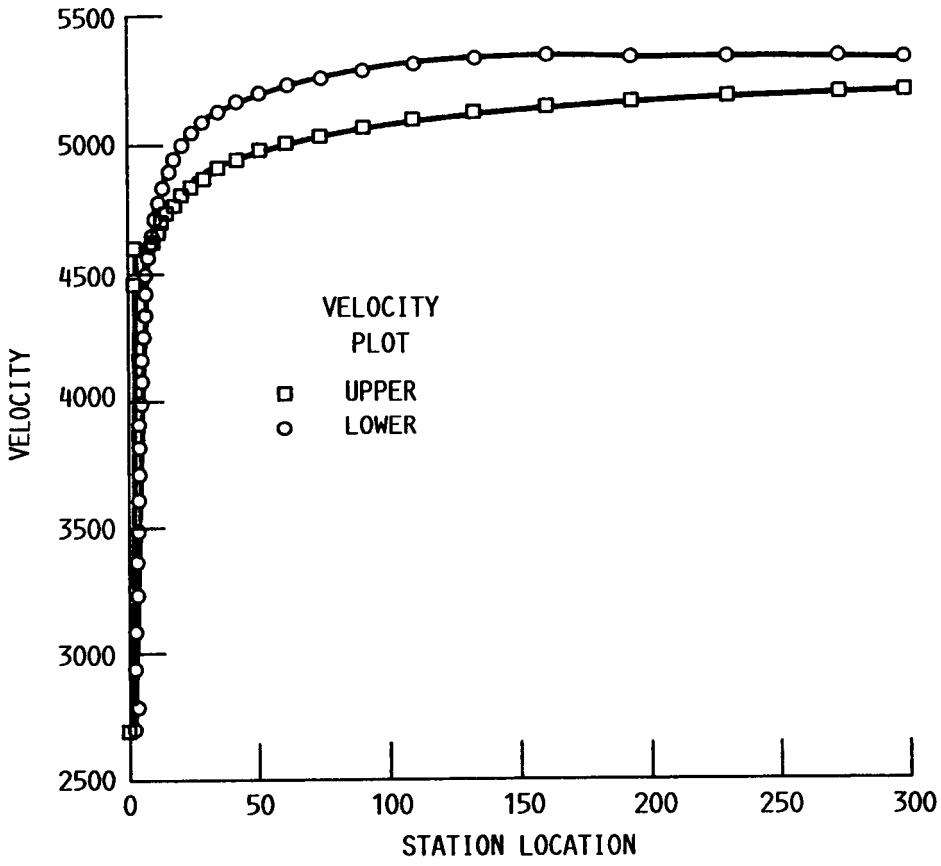

FIG. 20. - WALL AXIAL VELOCITY PLOT OF NONTRUNCATED NOZZLE

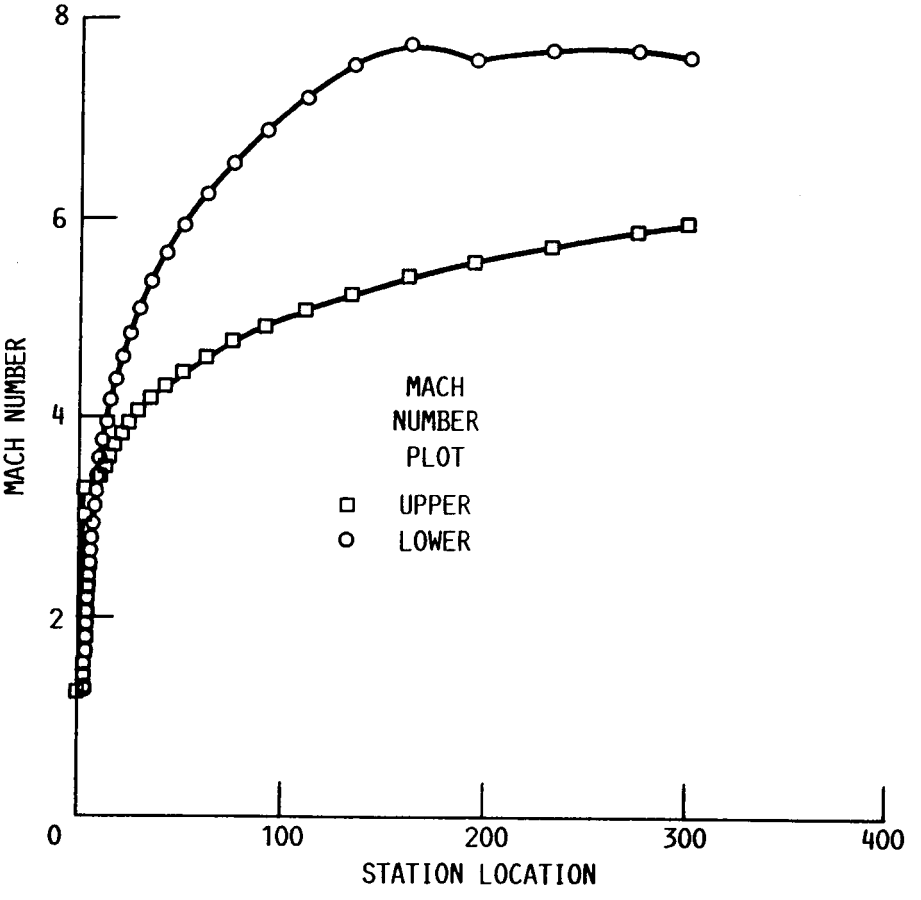

FIG. 21. - WALL AXIAL MACH NUMBER PLOT OF NONTRUNCATED NOZZLE

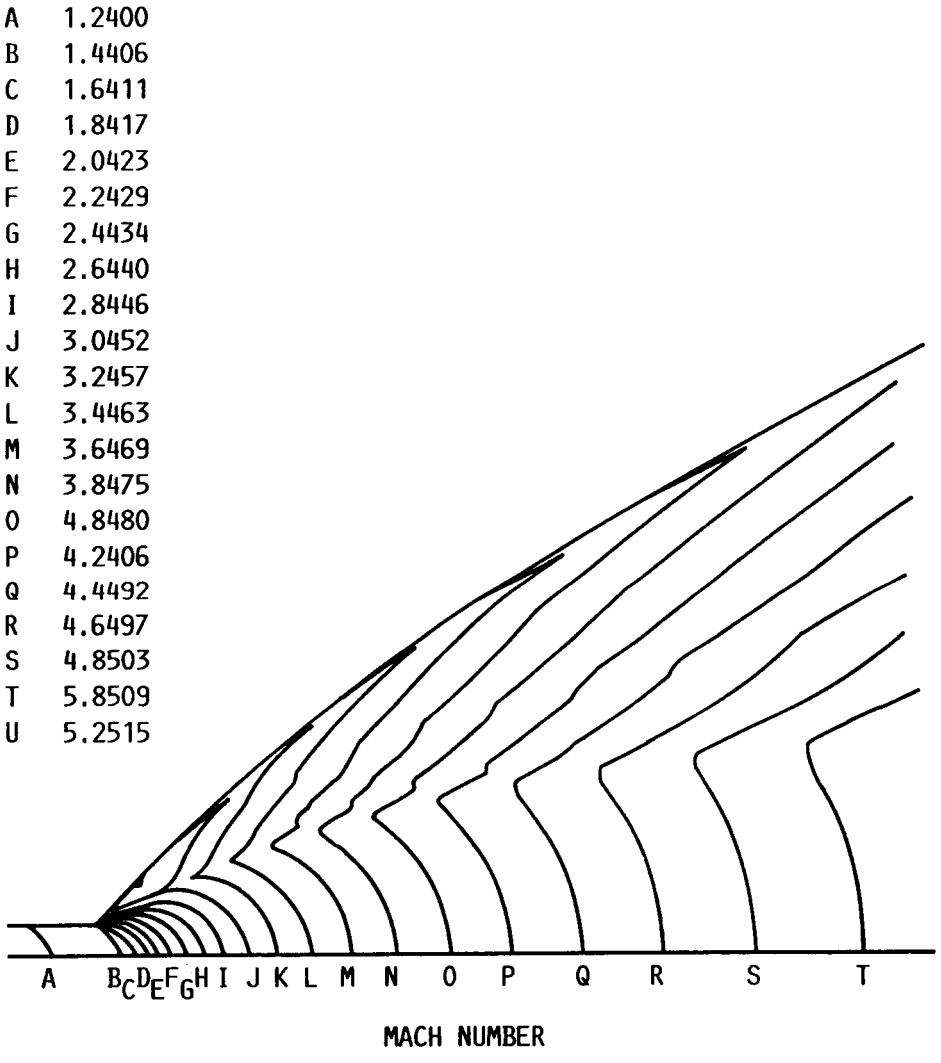

FIG. 22. - MACH NUMBER CONTOUR PLOT OF NONTRUNCATED NOZZLE

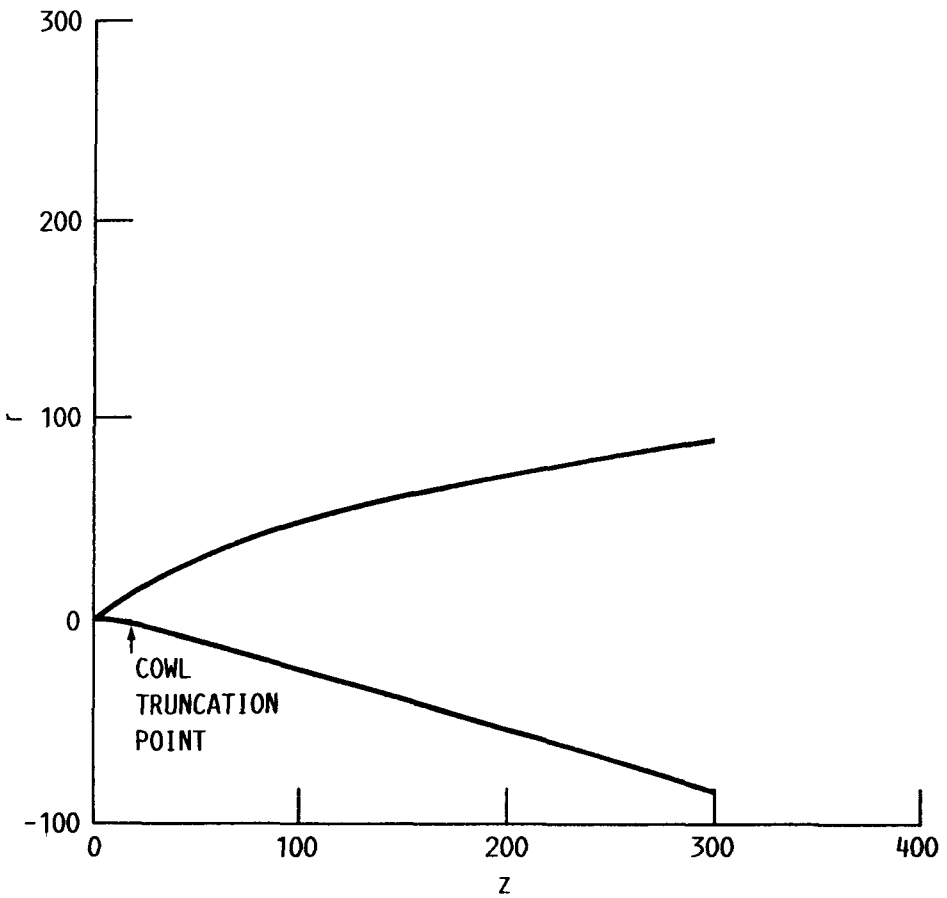

FIG. 23. - FLOW PATH GEOMETRY OF TRUNCATED SCARFED NOZZLE

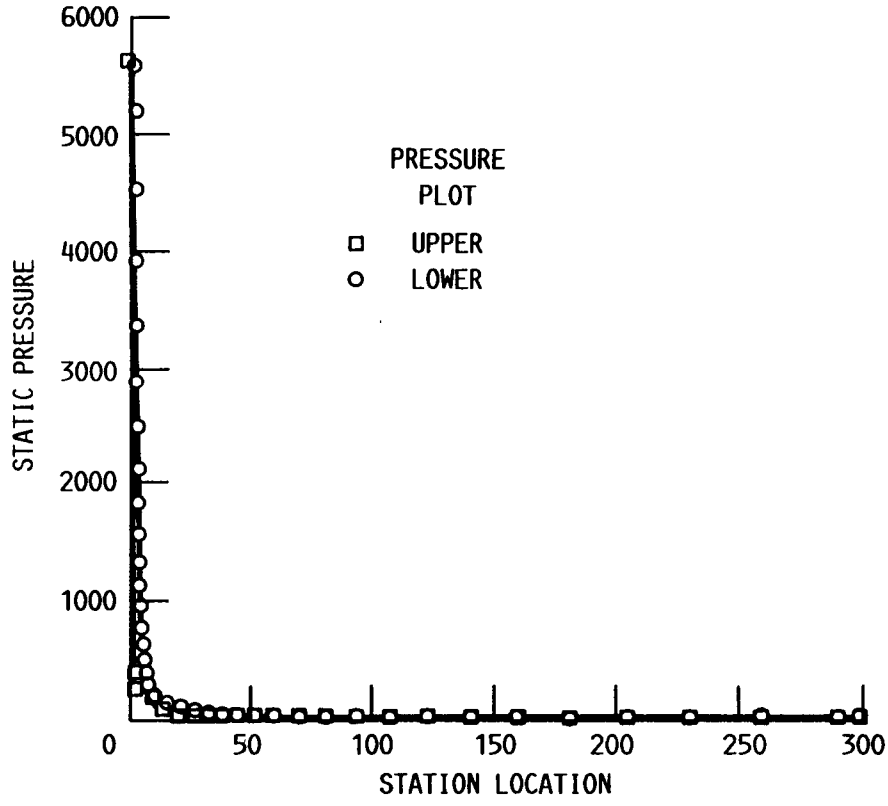

FIG. 24. - WALL STATIC PRESSURE PLOT OF TRUNCATED SCARFED NOZZLE

Figure 25 displays the computed axial velocity distribution. As exhibited in the static pressure distribution, the axial velocity drops to the freestream velocity after the truncation point. The Mach number distribution also displays a similar behavior and shows that the truncated scarfed nozzle does not internally expand as much as the nontruncated nozzle. This clearly illustrates the effect of the external flow on the expansion of the internal flow as shown in Fig. 26.

Figures 27 and 28 are plots of the oblique shock wave and slip line and Mach number contour for the truncated scarfed nozzle. Figure 27 displays the oblique shock wave and slip line emanating from the cowl truncation point. The slip line initially diverges from the internal flow and then converges as the effect of the external flow increases with nozzle length. The Mach number contour plot in Fig. 28 clearly illustrates the interaction of the external and internal flows. The slip line is depicted by the coalescing of contour lines in the center of the plot and the strength of the oblique shock wave is shown in the bottom portion of the figure. Also, the Prandtl-Meyer expansion fan interacts with the slip line in this case instead of the nozzle cowl wall in the nontruncated case.

Figure 29 is a comparison of nozzle ramp wall Mach Number distributions for the truncated scarfed nozzle. The Rao design and Seagull analysis compare very favorably except for the corner region where the compression wave occurs. This is illustrated by the jump in Mach Number at approximately 2.0 inches as shown in Fig. 29.

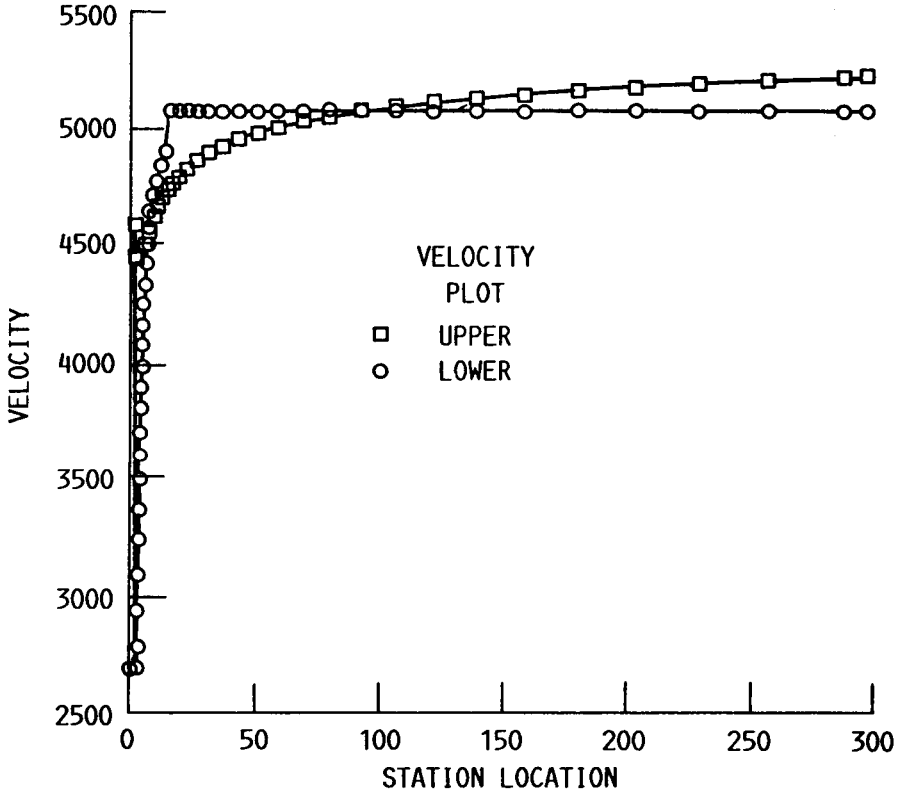

FIG. 25. - WALL AXIAL VELOCITY PLOT OF TRUNCATED SCARFED NOZZLE

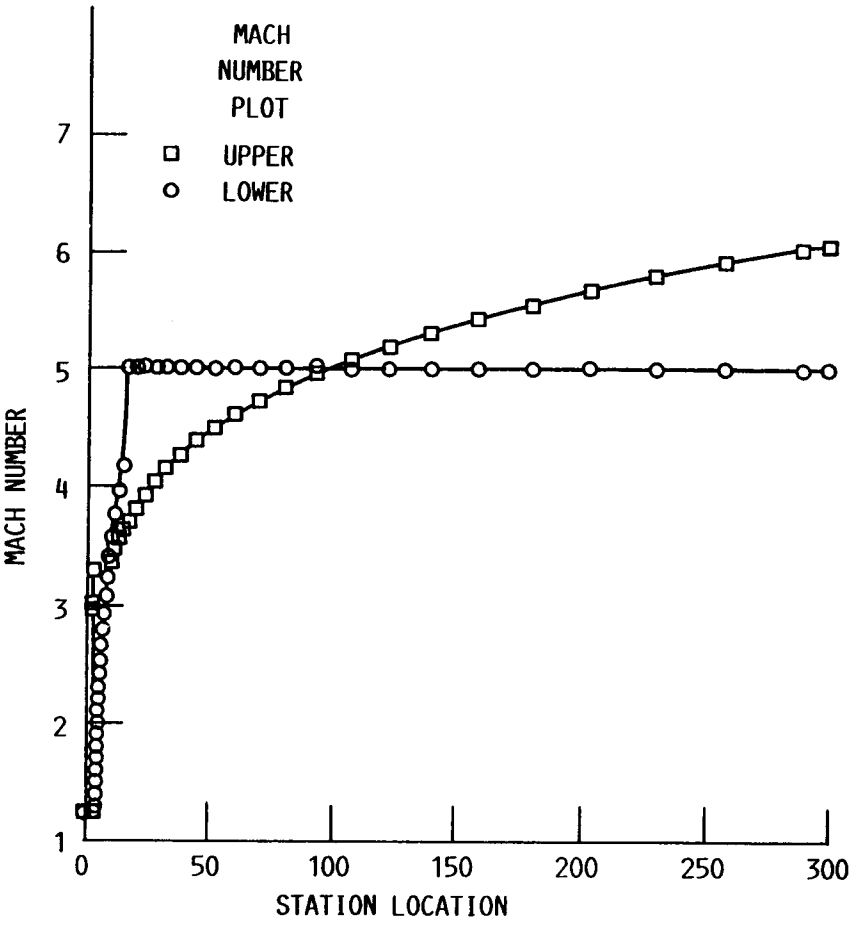

FIG. 26. - WALL AXIAL MACH NUMBER PLOT OF TRUNCATED SCARFED NOZZLE

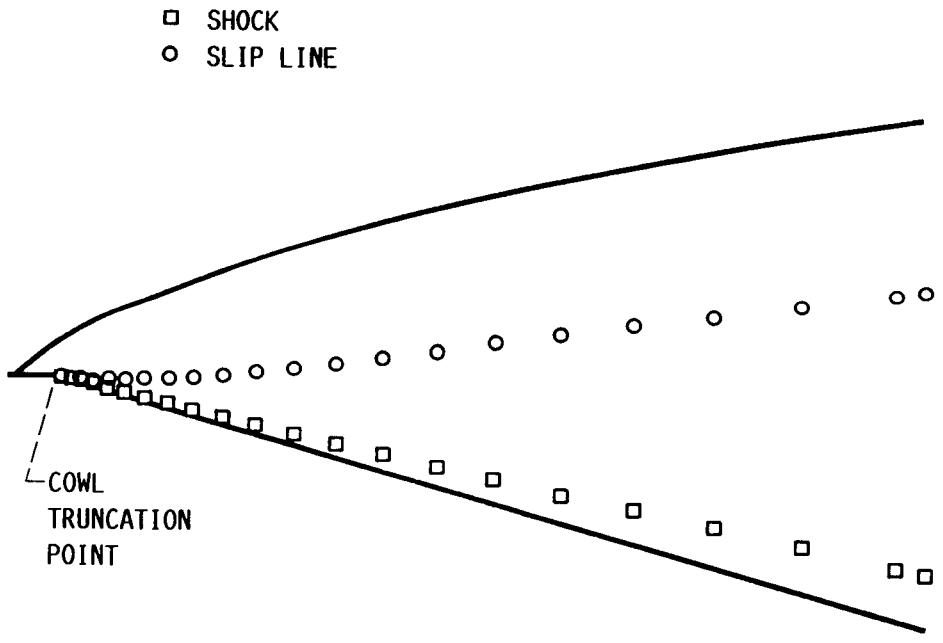

FIG. 27. - OBLIQUE SHOCK WAVE AND SHEAR LAYER PLOT OF TRUNCATED SCARFED NOZZLE

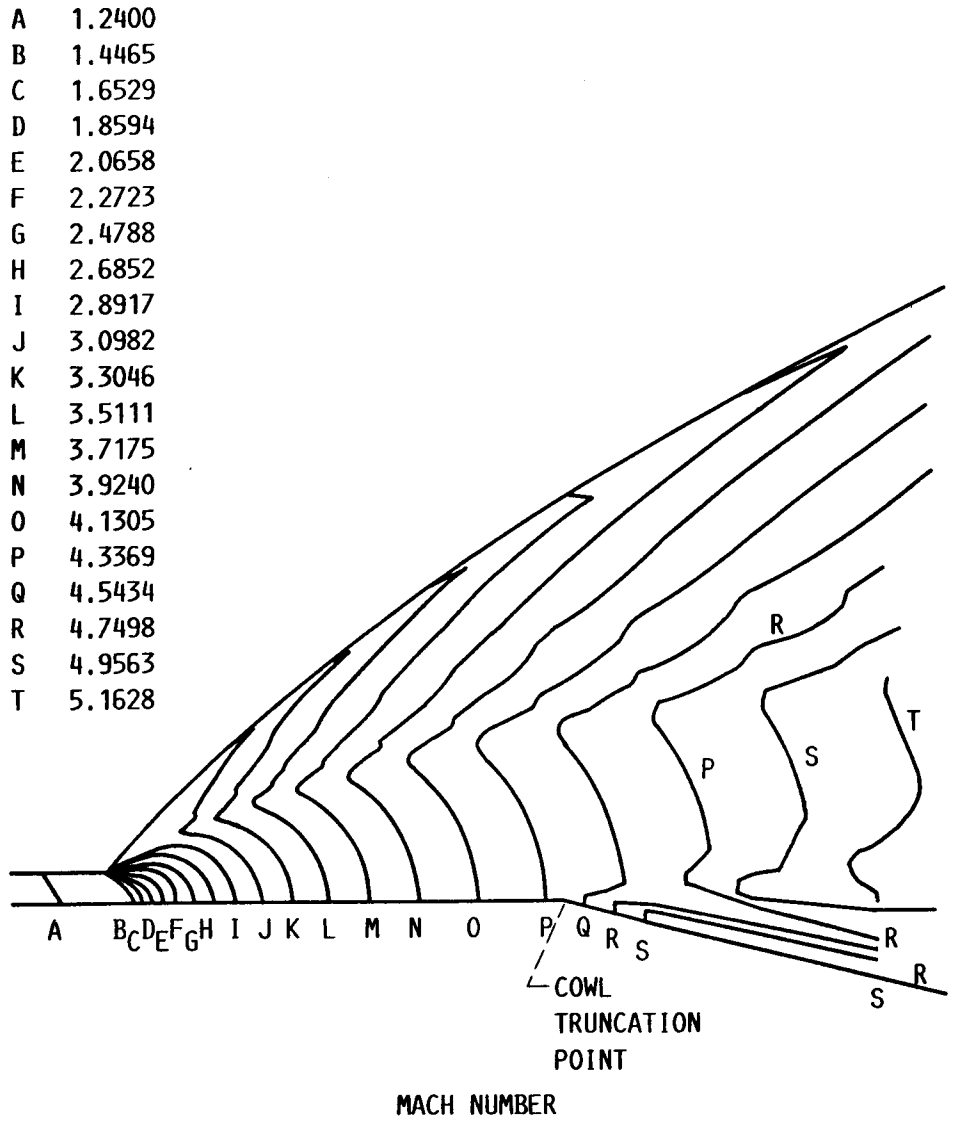

FIG. 28. - MACH NUMBER CONTOUR PLOT OF TRUNCATED SCARFED NOZZLE

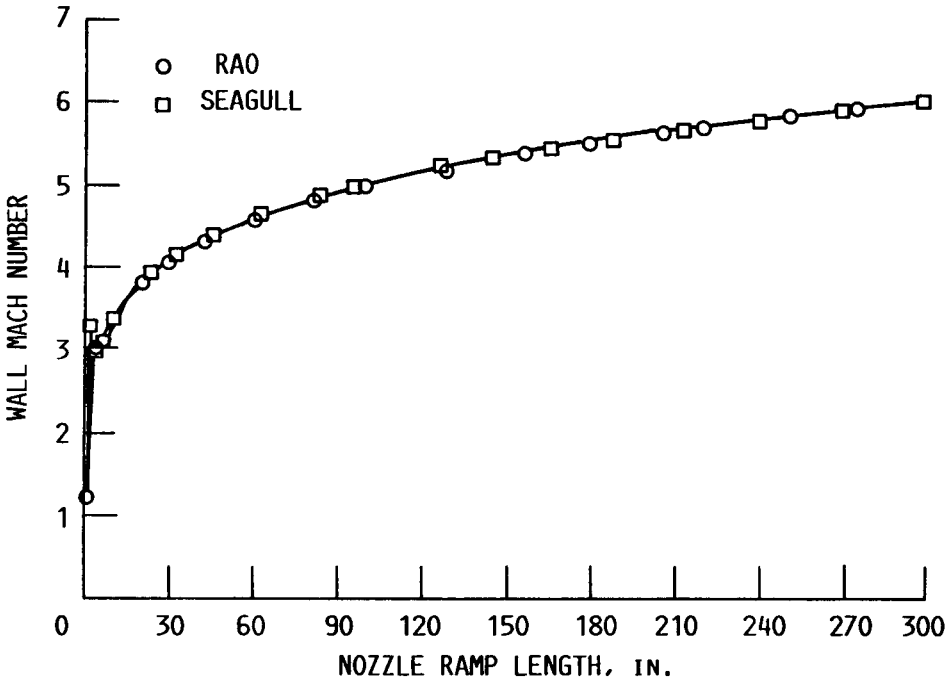

FIG. 29. - COMPARISON OF NOZZLE RAMP WALL MACH NUMBER DISTRIBUTIONS

CONCLUDING REMARKS

Results of a calculation of an optimized truncated scarfed nozzle were compared. The scarfed nozzle design showed less expansion than the nontruncated case and this was primarily due to the external flow affecting the internal flow expansion within the nozzle.

The comparison of thrust coefficient versus nozzle cowl length revealed that truncation of the cowl will affect the overall performance of an exhaust nozzle. This comparison demonstrates that there is an optimal cowl length in which truncation can be performed without degrading the overall nozzle performance. Truncation of the cowl past this optimal length should be analyzed in trade-off studies for thrust loss versus gross vehicle weight.

Plots of the oblique shock wave equations will allow the calculation of oblique shock wave and slip line angles, dynamic pressure coefficient, or ambient Mach number for various specific heat ratios. This will allow a designer to compute these flow quantities directly from the plots presented without use of the compressible flow equations.

The truncated scarfed nozzle method developed in this thesis can be extended in the future. The method can be modified to compute an optimum truncated scarfed nozzle with an oblique shock wave forming internally and simple chemical kinetics could also be incorporated into this method.

REFERENCES

1. Rao, G.V.R.: Exhaust Nozzle Contour for Optimum Thrust, Jet Propulsion, vol. 28, no. 6, June 1958, pp. 377-382.
2. Nickerson, G.R.: The Rao Method Optimum Nozzle Program, SEA Report No. 6/82/800.1, Software & Engineering Assoc., Santa Ana, CA, June 1982.
3. Shapiro, A.H.: The Dynamics and Thermodynamics of Compressible Fluid Flow. Vol. I, Ronald Press, New York, 1953.
4. John, J.E.A.: Gas Dynamics, 2nd edition, Allyn and Bacon Inc., Boston, MA, 1969.
5. Hildebrand, F.B.: Methods of Applied Mathematics, 2nd edition, Prentice-Hall, 1965.
6. Hildebrand, F.B.: Advanced Calculus for Applications, 2nd edition, Prentice-Hall, 1976.
7. Equations, Tables, and Charts for Compressible Fluid Flow. NACA Report 1135, 1953.
8. Zucrow, M.J. and Hoffman, J.D.: Gas Dynamics, Multi-dimensional Flow, vol. II, Robert E. Krieger Publishing Company, Malabar, FL, 1977.
9. Press, W.H., et al.: Numerical Recipes. Cambridge University Press, New York, 1986.

10. Salas, M.D.: Shock Fitting Method for Complicated Two-Dimensional Supersonic Flows, AIAA J., vol. 14, no. 5, May 1976, pp. 583-588.

APPENDIX A

LAGRANGIAN MULTIPLIERS

Situations occur in many engineering applications in which a function f is to be maximized or minimized dependent upon variables which are not independent of each other, but are interrelated by one or more constraint conditions.

The general case may be illustrated by the problem of maximizing or minimizing a function $f(x,y,z)$, so that $f(x,y,z)$ = relative max or min subject to two constraints of the form

$$g(x,y,z) = 0, \tag{A.1}$$

$$h(x,y,z) = 0, \tag{A.2}$$

where g and h are not functionally dependent, so that the constraints are neither equivalent nor compatible. It is assumed that the functions f, g, and h have first partial derivatives everywhere in a region which includes the desired critical point.

The function f is an extrememem at $P(x_o, y_o, z_o)$ if the linear terms in Taylor expansion of f about P are zero. This condition can be written in the form

$$f_x\, dx + f_y\, dy + f_z\, dz = 0 \quad \text{at} \quad (x_o, y_o, z_o). \tag{A.3}$$

However, the increments dx, dy, and dz are not independent, so it cannot be concluded that f_x, f_y, and f_z must vanish separately at

P. Since g and h are constant throughout the field, the differential of each must be zero at the point P, so that

$$g_x\,dx + g_y\,dy + g_z\,dz = 0 \quad \text{at} \quad (x_o, y_o, z_o) \tag{A.4}$$

$$h_x\,dx + h_y\,dy + h_z\,dz = 0 \quad \text{at} \quad (x_o, y_o, z_o). \tag{A.5}$$

Equations (A.4) and (A.5) are linear equations in dx, dy, and dz. These equations can be uniquely solved for two of the differentials in terms of a third if and only if g and h are functionally independent. By making use of Eqs. (A.4) and (A.5) two of the differentials (say dx and dy) can be eliminated from Eq. (A.3). This results in an equation of the form $F(x,y,z)\,dz = 0$, in which the one remaining differential can be arbitrarily assigned. In essence the conditions in Eqs. (A.4) and (A.5) along with the condition $F(x,y,z) = 0$ constitute a set of three equations in the three unknowns x_o, y_o, and z_o.

An alternative method of frequent usefulness, is based on the fact that one may multiply the equal members of Eqs. (A.4) and (A.5) by arbitrary constants, say, λ_1 and λ_2, respectively, and add the results to Eq. (A.3) to obtain the requirement that

$$(f_x + \lambda_1 g_x + \lambda_2 h_x)\,dx + (f_y + \lambda_2 g_y + \lambda_2 h_y)\,dy + (f_z + \lambda_1 g_z + \lambda_2 h_z)\,dz = 0 \tag{A.6}$$

at (x_o, y_o, z_o). This expression is valid for all values of λ_1 and λ_2. The latter which can now be determined so that the coefficients of two of the differentials are zero. If the preceding statement were not true, it would follow that

$$\begin{vmatrix} g_x & h_x \\ g_y & h_y \end{vmatrix} = \begin{vmatrix} g_y & h_y \\ g_z & h_z \end{vmatrix} = \begin{vmatrix} g_z & h_z \\ g_x & h_x \end{vmatrix} = 0$$

and hence g and h would be functionally dependent, so that the two constraints would be either equivalent or inconsistent. Assuming that λ_1 and λ_2 have been so determined, then the remaining differential can be arbitrarily assigned, so that its coefficient also must vanish. Thus, the three equations

$$\begin{aligned} f_x + \lambda_1 g_x + \lambda_2 h_x &= 0 \\ f_y + \lambda_1 g_y + \lambda_2 h_y &= 0 \quad \text{at} \quad (x_o, y_o, z_o) \\ f_z + \lambda_1 g_z + \lambda_2 h_z &= 0 \end{aligned} \tag{A.7}$$

along with the conditions

$$g = 0, \qquad h = 0 \quad \text{at} \quad (x_o, y_o, z_o) \tag{A.8}$$

comprise five equations in the five unknown quantities x_o, y_o, z_o, λ_1, and λ_2.

The parameters λ_1 and λ_2 are referred to as Lagrangian multipliers. If these parameters were eliminated from Eq. (A.6), the result would be the relation $F = 0$ obtained by eliminating dx, dy, and dz from Eqs.(A.3) to (A.5).

The relations in Eq. (A.7) provide the necessary conditions $\xi_x = 0$, $\xi_y = 0$, $\xi_z = 0$ so that the "auxillary function"

$$\xi = f + \lambda_1 g + \lambda_2 h \tag{A.9}$$

attains a relative maximum or minimum at (x_o, y_o, z_o) when no constraints are imposed.

The more general case would be if f were to be maximized subject to the restraints $g_1 = 0$, $g_2 = 0, \ldots, g_n = 0$. The auxillary function would then be

$$\xi = f + \lambda_1 g_1 + \lambda_2 g_2 \ldots + \lambda_n g_n, \qquad (A.10)$$

where $\lambda_1, \ldots, \lambda_2$ are unknown constants. The necessary conditions for rendering ξ a relative maximum or minimum with no constraints could be written and the solution could be subsequently determined.

Further explanation of the use of Lagrangian multipliers can be found in Hildebrand (1965 and 1976).

APPENDIX B

CALCULUS OF VARIATIONS

The calculus of variations is a mathematical procedure employed to determine one or more functions, subject to certain conditions, so as to maximize or minimize a specific definite integral, whose integrand depends upon the unknown function or functions and/or certain combination of their derivatives. The brief discussion of the theory of calculus of variations which follows is presented in greater detail in Hildebrand (1976).

To illustrate this method an example is considered. A case is considered in which we wish to maximize or minimize an integral of the form

$$I = \int_a^b F(x,u,u') \, dx, \tag{B.1}$$

subject to the conditions

$$u(a) = A, \; u(b) = B, \tag{B.2}$$

where a, b, A, and B are specified constants. The function F has continuous second-order derivatives with respect to its three arguments. It is further required that the unknown function $u(x)$ possess two derivatives everywhere in the interval (a, b).

Functions which have two derivatives in (a, b) and which take on the prescribed end values are admissible and out of all admissible

functions, a function (or functions) must be selected which makes I a maximum. Assuming there is one function $u(x)$ having the property above, a one-parameter family of admissible competing functions which includes $u(x)$, is first written as

$$u(x) + \varepsilon\eta(x)$$

where $\eta(x)$ is any arbitrary chosen twice-differentiable function which vanishes at the end points of the interval (a, b), i.e,

$$\eta(a) = \eta(b) = 0, \tag{B.3}$$

and where ε is a parameter which is constant for any one function in the set but which varies from one function to the next. The increment $\varepsilon\eta(x)$, representing the difference between the varied function and the actual solution function, is called a variation of $u(x)$.

Replacing $u(x)$ by $u(x) + \varepsilon\eta(x)$ in I yields another integral that is denoted by $I(\varepsilon)$,

$$I(\varepsilon) = \int_a^b F(x,u + \varepsilon\eta,u' + \varepsilon\eta') \, dx. \tag{B.4}$$

It then follows that $I(\varepsilon)$ takes on a maximum value when $\varepsilon = 0$, that is, when the variation of u is zero. Hence, it must follow that

$$\frac{dI(\varepsilon)}{d\varepsilon} = 0 \qquad \text{when} \qquad \varepsilon = 0. \tag{B.5}$$

The partial derivatives of F are assumed to be continuous with respect to its three arguments and this implies that the derivative $dF/d\varepsilon$ exists. Hence, $I(\varepsilon)$ under the integral sign may be differentiated to obtain

$$\frac{dI(\varepsilon)}{d\varepsilon} = \int_a^b \left[\frac{\partial F(x,u + \varepsilon\eta,u' + \varepsilon\eta')}{\partial(u + \varepsilon\eta)}\,\eta + \frac{\partial F(x,u + \varepsilon\eta,u' + \varepsilon\eta')}{\partial(u' + \varepsilon\eta')}\,\eta'\right]dx.$$

By setting $\varepsilon = 0$, an expression for the condition (B.5) is obtained, viz.,

$$\delta I'(0) = \int_a^b \left[\frac{\partial F}{\partial u}\,\eta(x) + \frac{\partial F}{\partial u}\,\eta'(x)\right]\,dx = 0 \qquad (B.6)$$

in which it is written that $F = F(x,u,u')$ and therefore the partial derivatives $\partial F/\partial u$ and $\partial F/\partial u'$ have been formed with x, u, and u' treated as independent variables.

Transforming the integral of the second product in Eq. (B.6) via an integration by parts yields

$$\int_a^b \frac{\partial F}{\partial u'}\,\eta'(x)\,dx = \left[\frac{\partial F}{\partial u'}\,\eta(x)\right]_a^b - \int_a^b \frac{d}{dx}\left(\frac{\partial F}{\partial u'}\right)\eta(x)\,dx$$

$$= -\int_a^b \frac{d}{dx}\left(\frac{\partial F}{\partial u'}\right)\eta(x)\,dx$$

as a consequence of Eq. (B.3). Equation (B.6) now becomes

$$\int_a^b \left[\frac{d}{dx}\left(\frac{\partial F}{\partial u'}\right) - \frac{\partial F}{\partial u}\right]\eta(x)\,dx = 0 \qquad (B.7)$$

It can be proven that, Eq. (B.7) is true for any function $\eta(x)$ which is twice differentiable in (a, b) and zero at the ends of that interval. Consequently, the coefficient of $\eta(x)$ in the integrand must be zero everywhere in (a, b), so that the condition

$$\frac{d}{dx}\left(\frac{\partial F}{\partial u'}\right) - \frac{\partial F}{\partial u} = 0 \qquad \text{(B.8)}$$

must be satisfied. This is called the Euler equation associated with the problem of maximizing or minimizing the integral in Eq. (B.1) subject to Eq. (B.2).

Recalling that F, and hence its partial derivatives, may depend upon x both directly and indirectly, through the intermediate variables $u(x)$ and $u'(x)$, it is deduced from the chain rule that

$$\frac{dM}{dx} = \frac{\partial M}{\partial x} + \frac{\partial M}{\partial u}\frac{du}{dx} + \frac{\partial M}{\partial u'}\frac{d^2u}{dx^2} \qquad \text{(B.9)}$$

where the function M may be identified with F or with one of its partial derivatives. Thus, in particular, we can employ $M = \partial F/\partial u'$ to write the Euler equation in an expanded form as

$$F_{u'u'}\frac{d^2u}{dx^2} + F_{uu'}\frac{du}{dx} + (F_{xu'} - F_u) = 0 \qquad \text{(B.10)}$$

The expanded form shows that when $F_{u'u'} = \partial^2 F/\partial u'^2$ is zero, the equation is in fact a differential equation of second order in u, subject to the two boundary conditions $u(a) = A$ and $u(b) = B$.

From Eq. (B.8) it follows that

$$\frac{\partial F}{\partial u'} = \text{constant} \qquad \text{when} \qquad F = F(x,u'), \qquad \text{(B.11)}$$

so that, when F does not involve u explicitly, the first-order equation $\partial F/\partial u' = \text{constant}$ comprises a "first integral" of the Euler equation. It can also be shown that Eq. (B.8) implies that

$$\frac{\partial F}{\partial u'} u' - F = \text{constant} \qquad \text{when} \qquad F = F(u,u'), \tag{B.12}$$

so that the first integral is also available when F does not involve x explicitly.

The equation above can be generalized to maximize or minimize an integral subject to a constraint condition. To maximize or minimize Eq. (B.1)

$$\int_a^b F(x,u,u')\, dx = \text{max or min}, \tag{B.13}$$

where $u(x)$ is to satisfy the prescribed end conditions

$$u(a) = A, \qquad u(b) = B, \tag{B.14}$$

as before, but that also a constraint condition is imposed in the form

$$\int_a^b G(x,u,u')\, dx = K, \tag{B.15}$$

where K is a prescribed constant. For this case, the appropriate Euler equation is found to be the result of replacing F in Eq. (B.8) by the auxiliary function

$$H = F + \lambda G \tag{B.16}$$

where λ is a Lagrangian multiplier and is equal to an unknown constant. This constant will generally appear in the Euler equation and in its solution. This constant has to be determined along with the two constants of integration in such a way that the three conditions of Eqs. (B.15) and (B.16) are satisfied.

APPENDIX C

SCARFED TRUNCATION POINT SUBROUTINE

A computer routine for determining the flow properties at the truncation point is presented of a two-dimensional nozzle is presented. The following equations are used in this analysis

$$\frac{P_T}{p} = \left[1 + \frac{\gamma - 1}{2} M^2\right]^{\gamma/\gamma-1} \tag{C.1}$$

$$\nu = \sqrt{\frac{\gamma + 1}{\gamma - 1}} \tan^{-1} \sqrt{\frac{\gamma - 1}{\gamma + 1}(M^2 - 1)} - \tan^{-1} \sqrt{M^2 - 1} \tag{C.2}$$

$$\cot \delta = \tan \theta \left[\frac{(\gamma + 1)M_1^2}{2(M_1^2 \sin^2\theta - 1} - 1\right] \tag{C.3}$$

$$\frac{p_2}{p_1} = \frac{2\gamma M_1^2 \sin^2\theta - (\gamma - 1)}{\gamma + 1} \tag{C.4}$$

These equations are used to compute static and total pressure, Mach number, slip line angle, oblique shock wave angle, and Prandtl-Meyer expansion angle at the scarfed truncation point. These flow relations can be used to analyze the flow phenomena at the truncation point. The truncation point and flow phenomena described previously is schematically shown in Fig. C1. A computer flow diagram is presented in Fig. C2. The listing of the computer program is also provided.

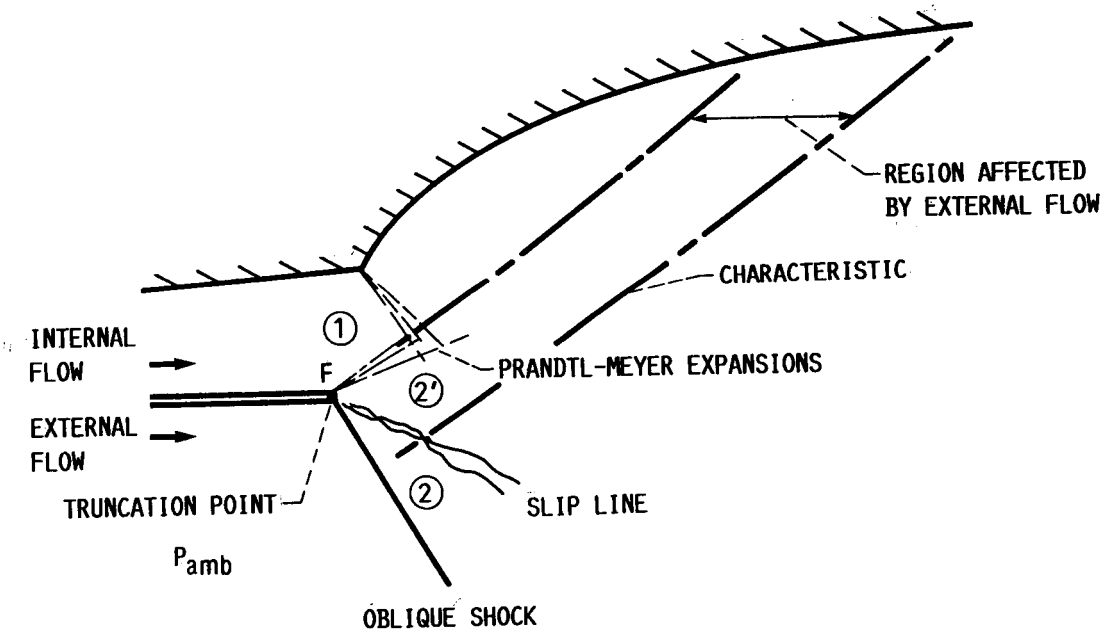

FIG. C1. - SCHEMATIC OF TRUNCATED TWO-DIMENSIONAL RAO NOZZLE

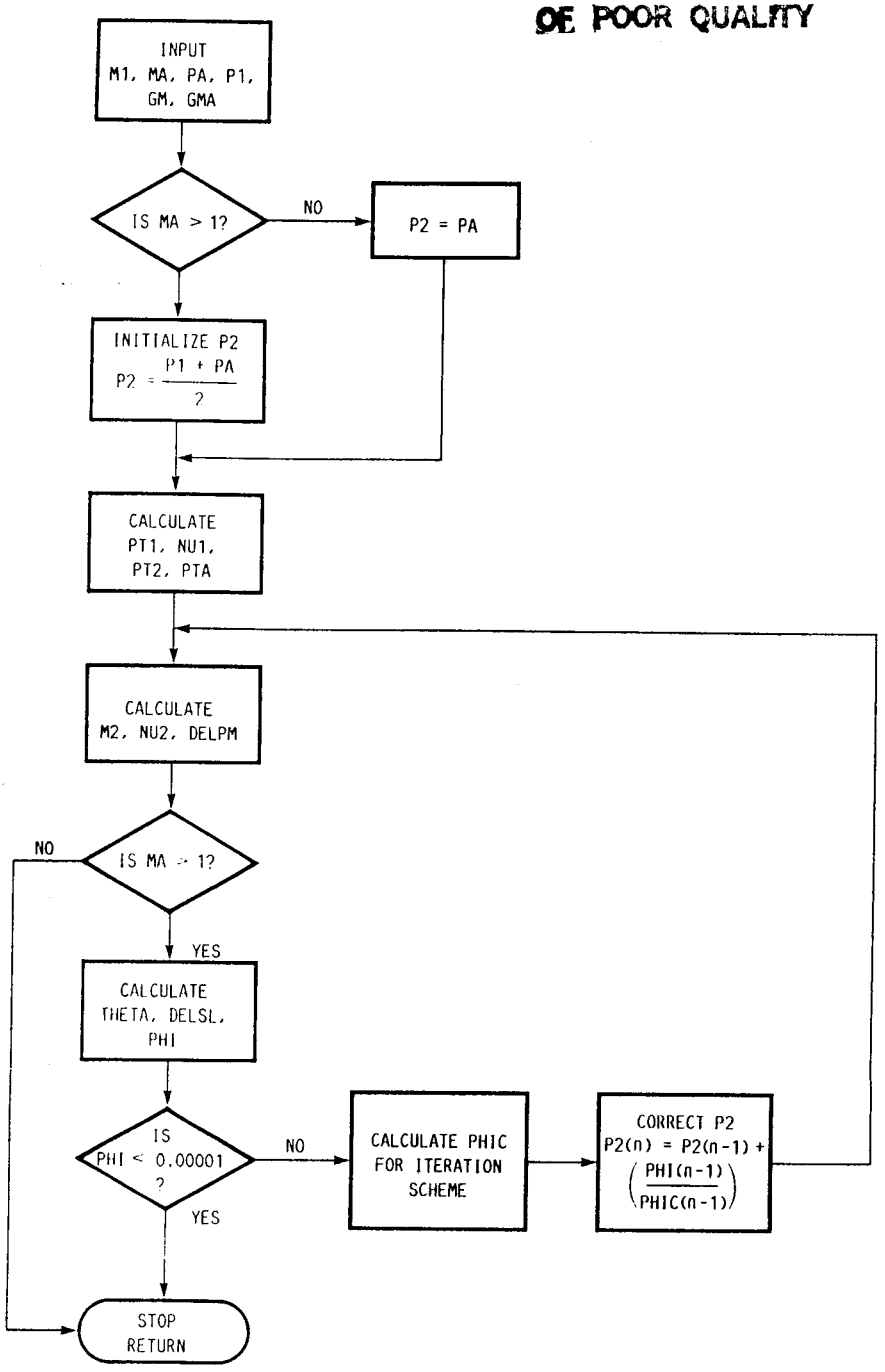

FIG. C2. - COMPUTER FLOW DIAGRAM OF SCARFED TRUNCATION SUBROUTINE

```
0000100 C
0000200 C...THIS ROUTINE COMPUTES THE FLOW QUANTITIES REQUIRED FOR THE SCARFED
0000300 C...NOZZLE OPTIMTIZATION
0000400 C
0000500       REAL NU1,NU2(200),M1,M2(200),MA,P1,P2(200),PA,PT1,PT2,PTA
0000600       REAL GM,GMA,DELSL(200),DELPM(200),THETA(200),PHI(200),PHIC(200)
0000700       REAL DNU2DM(200),DDLDTH(200),DP2DM2(200),DP2DTH(200)
0000800       REAL A,B,X,Y,Z,F,G,H
0000900       REAL PR1,PR2,PR3,PR4,PR5
0001000       READ(5,10,END=1) M1,MA,PA,GM,GMA
0001100    10 FORMAT(5(F12.5/))
0001200     1 I=1
0001300    77 READ(5,11) P1
0001400    11 FORMAT(F10.5)
0001500       IF( P1 .EQ. 1.0 ) GO TO 30
0001600       IF( MA .GT. 0.0) GO TO 15
0001700       GO TO 20
0001800 C
0001900 C...INITIALIZE STATIC PRESSURE AT STATE 2, P2
0002000 C
0002100    15 P2(I)=(P1+PA)/2.
0002200       GO TO 25
0002300    20 P2(I)=PA
0002400 C
0002500 C...CALCULATE THE TOTAL PRESSURE AT STATE 1
0002600 C
0002700    25 PT1=P1*((1.+ (GM-1.)/2. *(M1**2.0))**(GM/(GM-1.)))
0002800 C
0002900 C...CALCULATE THE PRANDTL-MAYER ANGLE NU, AT STATE 1
0003000 C
0003100       NU1=(SQRT ((GM+1.)/(GM-1.)) ) * ATAN( SQRT((GM-1.)/(GM+1.)*   -
0003200      $(M1**2.-1.)) ) - ATAN( SQRT(M1**2.-1.) )
0003300       PT2=PT1
0003400 C
0003500 C...CALCULATE THE MACH NUMBER AT STATE 2
0003600 C
0003700    35 M2(I)=SQRT( ( (PT2/P2(I))**((GM-1.)/GM ) -1.) * (2./(GM-1.)) )
0003800 C
0003900 C...CALCULATE THE PRANDTL-MAYER ANGLE NU, AT STATE 2
0004000 C
0004100     3 NU2(I)=SQRT( (GM+1.)/(GM-1.)) * ATAN( SQRT( ((GM-1.)/(GM      -
0004200      $+1.))*(M2(I)**2.-1.) ) ) - ATAN( SQRT(M2(I)**2.-1.) )
0004300 C
0004400 C...CALCULATE THE TOTAL PRANDTL-MAYER ANGLE, DELPM
0004500 C
0004600       DELPM(I)=NU2(I)-NU1
```

```
0004700 C
0004800 C...CALCULATE THE AMBIENT TOTAL PRESSURE
0004900 C
0005000       PTA=PA*((1.+(GMA-1.)/2.*(MA**2.))**(GMA/(GMA-1.)))
0005100 C
0005200 C...CALCULATE THE SHOCK WAVE ANGLE, THETA
0005300 C
0005400       THETA(I)=ARSIN( SQRT(((P2(I)/PA)*(GMA+1.)+(GMA-1.))/(2.*GMA  -
0005500      $*MA**2.)) )
0005600 C
0005700 C...CALCULATE THE SLIP LINE ANGLE, DELSL
0005800 C
0005900       A=(GMA+1.)*MA**2.
0006000       B=2.*( MA**2.*(SIN(THETA(I))**2.) - 1. )
0006100       DELSL(I)=ATAN( 1./( TAN(THETA(I))*(A/B - 1.) ) )
0006200 C
0006300 C...CALCULATE PHI FOR ITERATION SCHEME
0006400 C
0006500       PHI(I)=( DELPM(I) -  DELSL(I) )
0006600 C
0006700 C...CHECK PHI FOR CONVERGENCE
0006800 C
0006900       IF( ABS( PHI(I) ) .LT. 0.000001 ) GO TO 30
0007000 C
0007100 C...COMPUTE DERIVATIVES FOR ITERATION SCHEMES
0007200 C
0007300
0007400       DNU2DM(I)=SQRT( (M2(I)**2.-1.0) ) /( M2(I)**3.*((GM-1.)/2.)   -
0007500      $+ M2(I) )
0007600       DP2DTH(I)=( 4.*GMA*MA**2.*PA*SIN(THETA(I))*COS(THETA(I)) )/   -
0007700      $(GMA + 1.)
0007800       X=-1./( 2.*SIN(THETA(I))*COS(THETA(I)) )
0007900       Y=( 2.*MA**2.*SIN(THETA(I))*COS(THETA(I)) )/( MA**2.*SIN(     -
0008000      $THETA(I))**2.-1. )
0008100       Z=( 4.*MA**2.*SIN(THETA(I))*COS(THETA(I)) )/( 2.+MA**2.*(     -
0008200      $(GMA+1.) - 2*( SIN(THETA(I)))**2.) )
0008300       DDLDTH(I)=SIN(DELSL(I)) * COS(DELSL(I)) * ( X+Y+Z )
0008400       DP2DM2(I)=-( GM*M2(I)*P2(I) )/( 1.+(GM-1.)*0.5*M2(I)**2. )
0008500 C
0008600 C...CALCULATE CAP PHI
0008700 C
0008800       PHIC(I)=( DNU2DM(I)/DP2DM2(I) - DDLDTH(I)/DP2DTH(I) )
0008900       N=I+1
0009000    5  P2(N)=P2(I) - PHI(I)/PHIC(I)
0009100 C
0009200 C...INDEX COUNTER
```

```
0009300 C
0009400       I=I+1
0009500       GO TO 35
0009600 C
0009700 C...CONVERT ANGLES TO DEGREES
0009800 C
0009900    30 DELSL(I)=DELSL(I)*(1/0.01745239)
0010000       DELPM(I)=DELPM(I)*(1/0.01745239)
0010100       NU1=NU1*(1/0.01745239)
0010200       NU2(I)=NU2(I)*(1/0.01745239)
0010300       PR1=PA/PTA
0010400       PR2=P1/PA
0010500       PR3=PTA/PT1
0010600       PR4=PT1/P1
0010620       PR5=P2(I)/PA
0010700 C
0010800 C...WRITE FLOW QUANTITIES COMPUTED
0010900 C
0011000       WRITE(6,50) NU1,M1,PT1,MA,PTA,I
0011100    50 FORMAT(6F10.5,I3,//)
0011200       WRITE(6,60) P2(I),M2(I),DELSL(I),DELPM(I),NU2(I)
0011300    60 FORMAT(5F10.5,/)
0011400       WRITE(7,70) P2(I),M2(I),DELSL(I),DELPM(I),NU2(I),                -
0011500      $NU1,M1,P1,PT1,MA,PA,PTA,GM,GMA,I
0011600    70 FORMAT(//,'P2=',F10.5,5X,'M2=',F10.5,5X,'DELSL=',F10.5,//,      -
0011700      $'DELPM=',F9.5,3X,'NU2=',F10.5,4X,'NU1=',F10.5,//,'M1=',         -
0011800      $F10.5,5X,'P1=',F10.5,5X,'PT1=',E10.5,//,'MA=',F10.5,5X,'PA=', -
0011900      $F10.5,5X,'PTA=',E10.5,//,'GM=',F10.5,5X,'GMA=',F10.5,4X,'I=',I3)
0012000       WRITE(8,80) PR2,PR3,NU1,NU2(I),DELSL(I),MA,PA,M1,PT1,PTA
0012100    80 FORMAT(10F11.3)
0012200       WRITE(9,89) PR2,PR5,DELSL(I)
0012300    89 FORMAT(3F11.3)
0012400    99 STOP
0012500       END
EOF
```

NASA
National Aeronautics and Space Administration

Report Documentation Page

1. Report No.	2. Government Accession No.	3. Recipient's Catalog No.
NASA TM-100955		

4. Title and Subtitle	5. Report Date
Analysis and Optimization of Truncated Scarf Nozzles Subject to External Flow Conditions	August 1988
	6. Performing Organization Code

7. Author(s)	8. Performing Organization Report No.
Rickey J. Shyne	E-4146
	10. Work Unit No.

9. Performing Organization Name and Address	11. Contract or Grant No.
National Aeronautics and Space Administration Lewis Research Center Cleveland, Ohio 44135-3191	
	13. Type of Report and Period Covered
12. Sponsoring Agency Name and Address	Technical Memorandum
National Aeronautics and Space Administration Washington, D.C. 20546-0001	14. Sponsoring Agency Code

15. Supplementary Notes

This report was a thesis submitted in partial fulfillment of the requirements for the degree of Master of Science in Mechanical Engineering to the University of Toledo, Toledo, Ohio in June 1988.

16. Abstract

Results of a calculation of an optimized truncated scarfed nozzle were compared. The truncated scarfed nozzle was designed for an exit Mach number of 6.0, i.e., the Mach number at the last nozzle characteristic is 6.0, with an external flow Mach number of 5.0. The nozzle was designed by the Rao method for optimum thrust nozzles modified for two-dimensional flow and truncated scarfed nozzle applications. This design was analyzed using a shock-fitting method for two-dimensional supersonic flows. Excellent agreement was achieved between the design and analysis. Truncation of the lower nozzle wall (cowl) revealed that there is an optimum length for truncating the cowl without degrading the nozzle performance. Truncation of the nozzle cowl past this optimal length should be analyzed in trade-off studies for thrust loss versus gross vehicle weight. Plots of the oblique shock wave equations were also identified which will allow computation of slip line angle, dynamic pressure coefficient, or ambient Mach number for various specific heat ratios.

17. Key Words (Suggested by Author(s))	18. Distribution Statement
Nozzle; Scarf; Optimization; Method of characteristics; Truncated; External flow effects	Unclassified - Unlimited Subject Category 02

19. Security Classif. (of this report)	20. Security Classif. (of this page)	21. No of pages	22. Price*
Unclassified	Unclassified		

NASA FORM 1626 OCT 86

*For sale by the National Technical Information Service, Springfield, Virginia 22161